Nitrosyl-Centered Redox and Acid−Base Interconversions in [Ru(Me₃[9]aneN₃)(bpy)(NO)]$^{3,2,1+}$. The pK_a of HNO for its Nitroxyl Derivative in Aqueous Solution

Nicolás Osa Codesido,[†] Thomas Weyhermüller,[‡] José A. Olabe,[†] and Leonardo D. Slep*,[†]

[†]Departamento de Química Inorgánica, Analítica y Química Física, Facultad de Ciencias Exactas y Naturales, and INQUIMAE, Universidad de Buenos Aires - CONICET, Pabellón 2, 3er piso, Ciudad Universitaria, C1428EHA Ciudad Autónoma de Buenos Aires, Argentina

[‡]Max Planck Institute for Chemical Energy Conversion, Stiftstraße 34-36, D-45470 Mülheim an der Ruhr, Germany

Ⓢ *Supporting Information*

ABSTRACT: This work reports the preparation of a new 6-coordinated nitrosyl compound and its use as a model to explore the redox and acid−base properties of the three redox states of bound nitrosyl (formally NO$^+$, NO$^•$, NO$^-$/HNO) in {RuNO}^{6,7,8} species. We prepared the octahedral {RuNO}^{6} complex [Ru(Me₃[9]aneN₃)(bpy)(NO)]$^{3+}$ (Me₃[9]aneN₃: 1,4,7-trimethyl-1,4,7-triazacyclononane; bpy = 2,2′-bipyridine), and the related [Ru(Me₃[9]-aneN₃)(bpy)(NO₂)]$^+$ nitro derivative. The compounds were characterized by chemical analysis, X-ray diffraction, NMR, IR, and UV−vis spectroscopies, cyclic voltammetry (CV), UV−vis/IR spectroelectrochemistry, and theoretical calculations (DFT, (TD)DFT). The reaction kinetics between the {RuNO}^{6} complex and the nucleophile OH$^-$ is also presented. The incorporation of tridentate and bidentate ligands in the coordination sphere prevents labilization issues associated with the trans effect when attaining the reduced states of the nitrosyl group. This allows for a consistent interpretation of the changes in the main geometrical parameters: Ru−N and N−O distances, Ru−N−O angle, and the ν_{NO} frequency and electronic transitions. We explore the redox properties in acetonitrile and aqueous solutions, and provide a potential ($E_{1/2}$) − pH (Pourbaix) diagram for the three diatomic nitrosyl-bound species, as well as for HNO and NO₂$^-$, including the report of the pK_a of the [Ru(Me₃[9]aneN₃)(bpy)(HNO)]$^{2+}$ ion, 9.78 ± 0.15 at 25.0 °C.
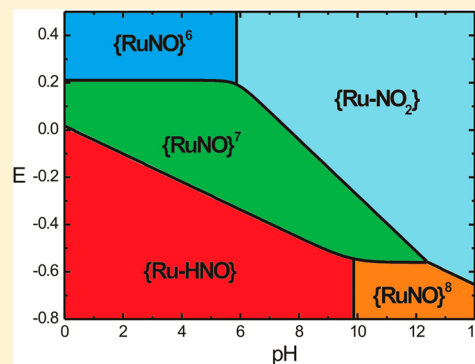
INTRODUCTION

Nitric oxide (NO) chemistry has remained an attractive topic to the inorganic chemistry community for several decades due to the enormous variety of coordination modes, spectroscopic properties, and reactivities displayed by nitrosyl-containing coordination compounds.[1−4] The number of publications and citations regarding transition metallonitrosyl chemistry increased significantly in the last years once the physiological role of nitric oxide was unraveled.[5] As a biological mediator NO engages most frequently in processes that require the interaction with heme proteins.[5] Thus, the biosynthetic route for NO starting from L-arginine and catalyzed by NO synthase[6] and the binding of NO to guanylate cyclase for promoting vasodilation[7] are two representative examples of specialized functional roles for NO in biochemistry. Also, 1-electron redox changes of bound nitrosyl species occur in diverse instances of denitrification.[8] This is the case for the processes involving a full 6-electron conversion of NO₂$^-$ into NH₃, catalyzed by the assimilatory nitrite reductase enzymes, or in the reduction of NO₂$^-$ to NO effected by the dissimilatory nitrite reductases.[9,10] This kind of (bio)chemistry, including also the NO reductases catalyzing the NO → N₂O conversion,[9,10] explains the early interest in the coordination chemistry of NO and its redox-related partners, the nitrosonium cation (NO$^+$) and the nitroxyl anion (NO$^-$). The observed different physiological roles of NO and HNO/NO$^-$ in animal and plant physiology added a new focus on the studies of reduced nitrosyl complexes,[11] looking for the elucidation of the basic chemistry under biorelevant conditions.[12,13] Recent reviews account for the significant progress achieved in the synthesis of metalloporphyrins holding bound NO and HNO/NO$^-$, with focus on their electronic structure, function, and reactivity in relation to biological systems.[14,15]

All three diatomic moieties have been successfully identified in coordination compounds of d^6 metal centers.[4] The chemistry of {MNO}^{6} complexes[16,17] is nowadays reasonably well understood, although this is not the case with the fewer well-characterized {MNO}^{7} complexes.[2,4] While the 6-coordinated {MNO}^{8} (heme and nonheme) complexes are scarce,[18−24] early[25] and more recent focus has been placed on the preparation and detailed spectroscopic characterization of low-spin 5-coordinated {FeNO}^{8} porphyrin model complexes, relevant to biological NO reduction. These species can be

handled in organic solvents and provide access to the 5-coordinated HNO derivatives upon acidification.[26−28] A limited collection of 6-coordinated complexes containing HNO[29−31] or its conjugate base NO−,[19−24,32−35] based on metals of the three transition series, has been obtained and structurally characterized. In general terms the consensus for many years has been that these species are short-lived in solution, precluding any attempt to characterize them from the reactivity point of view.[13] In addition, most of them have been reported as soluble only in organic solvents, with the remarkable exception of the HNO derivative of myoglobin, Mb(HNO),[36] and of [Fe(CN)$_5$(HNO)]$^{3−}$.[37] The situation is markedly different with free ^{1}HNO, where the first report on its acid−base properties can be traced back to the 1970s, indicating a pK_a value of 4.7.[38] The latest publications suggest that the pK_a is close to 11.5 (leading to free ^{3}NO−) or 23 (yielding ^{1}NO−).[39] Not long ago [Fe(CN)$_5$(NO)]$^{2−}$ was shown to undergo two consecutive one-electron reductions with S$_2$O$_4^{2−}$ to generate the HNO complex [Fe(CN)$_5$(HNO)]$^{3−}$ in aqueous solution.[37] This species appears to be reducing in basic medium but can be handled reasonably well in the neutral pH range without significant HNO-redox or -dissociation chemistry.[40] Analysis of the pH dependence of the ^{1}H NMR HNO signal at 20.32 ppm yielded the first report of the pK_a of coordinated HNO, which turned out to be 7.7.[37] This unprecedented (and still unique) experimental determination prompts several questions concerning the identity and redox chemistry of metallonitroxyl species. Are they rare examples of highly reactive molecules? Is it possible to handle NO−/HNO coordinated to metal centers long enough in aqueous solution so as to perform systematic studies of electronic structure and reactivity? Can their properties be rationalized and eventually fine-tuned? In this contribution we go a step further on these and other questions. We describe the preparation of a stable {MNO}^{6} compound that renders the desired $n = 7$ and 8 partners by consecutive one-electron reduction processes in acetonitrile *and water*. Following an exhaustive characterization, we explore the acid−base behavior of the coordinated nitrosyl at the different redox levels.

■ EXPERIMENTAL SECTION

Materials and Reagents. The reagents employed in the synthetic procedures were purchased from Sigma-Aldrich, and were used without further purification. All the organic solvents employed in synthetic procedures or physical determinations were dried and freshly distilled before use following standard procedures.[41] A vacuum line and Schlenk glassware (or alternatively a glovebox) were employed when the manipulation required exclusion of air.

Synthesis of the Compounds. *[Ru(Me$_3$[9]aneN$_3$)(bpy)(NO$_2$)]-ClO$_4$, [1](ClO$_4$).* A total of 70 mg of [Ru(Me$_3$[9]aneN$_3$)(bpy)(OH$_2$)]-(ClO$_4$)$_2$[42] (0.11 mmol) and 145 mg of NaNO$_2$ (2.10 mmol) were suspended in 20 mL of water. The dark-red mixture was refluxed for 1 h under Ar, yielding an orange solution. The reaction mixture was then treated with 1 mL of 0.1 M NaOH before reducing the volume in a rotary evaporator down to 5 mL. At this moment 132 mg of NaClO$_4$ (1.08 mmol) were added, and the solution was allowed to stand overnight at 4 °C. The red solid was collected by filtration, washed with cold water, and dried. The product was dissolved in 5 mL of 10$^{−3}$ M NaOH, and allowed to evaporate slowly at room temperature. The orange microcrystals were collected, washed with cold water, and dried in a vacuum. Yield: 48 mg (77%). Anal. Calcd for [1](ClO$_4$), C$_{19}$H$_{29}$N$_6$ClO$_6$Ru (MW: 574.00 g mol$^{−1}$): C, 39.8; H, 5.1; N, 14.6. Found: 39.2; H, 5.7; N, 14.4. IR (KBr pellet): ν_{asym}, 1300 cm$^{−1}$; ν_{sym}, 1265 cm$^{−1}$; δ_{ONO}, 769 cm$^{−1}$; ρw$_{(NO_2)}$, 623 cm$^{−1}$. UV–vis: λ_{max}/nm (ε/ M$^{−1}$ cm$^{−1}$), in H$_2$O: 446 (3.6 × 10^3), 366 (4.4 × 10^3), 294 (2.4 × 10^4),

256 (sh) (7.1 × 10^3), 238 (9.8 × 10^3); in CH$_3$CN: 480 (3.6 × 10^3), 338 (sh) (4.1 × 10^3), 296 (1.8 × 10^4), 258 (sh) (6.3 × 10^3), 244 (1.0 × 10^4). ^{1}H NMR (CD$_3$CN, δ/ppm): 9.18 (dd, 2H, $J_{\alpha\beta}$ = 6 Hz, $J_{\alpha\gamma}$= 1.4 Hz, H$_\alpha$), 8.43 (dd, 2H, $J_{\sigma\gamma}$ = 8 Hz, $J_{\sigma\beta}$ = 1.4 Hz, H$_\sigma$), 8.02 (ddd, 2H, $J_{\gamma\sigma}$ = 8 Hz, $J_{\gamma\beta}$ = 7.4 Hz, $J_{\gamma\alpha}$ = 1.4 Hz, H$_\gamma$), 7.54 (ddd, 2H, $J_{\beta\gamma}$ = 7.4 Hz, $J_{\beta\alpha}$= 6 Hz, $J_{\beta\sigma}$ = 1.4 Hz, Hβ), 3.57 (m, 2H, H$_{CH_2}$), 3.25 (m, 2H, H$_{CH_2}$), 3.11 (s, 6H, H$_x$), 3.03 (m, 2H, H$_{CH_2}$), 2.95 (m, 2H, H$_{CH_2}$), 2.89 (m, 2H, H$_{CH_2}$), 2.80 (m, 2H, H$_{CH_2}$), 1.78 (s, 3H, Hy); ^{13}C NMR (CD$_3$CN, δ/ppm): 161.50 (C$_\pi$), 153.91 (C$_\alpha$), 137.36 (C$_\gamma$), 125.91 (C$_\beta$), 123.96 (C$_\sigma$), 61.96 (CH$_2$), 60.44 (CH$_2$), 60.40 (CH$_2$), 53.95 (CH$_3$), 51.98 (CH$_3$). Slow diffusion of diethyl ether onto an acetonitrile solution of [1](ClO$_4$) yielded deep-red single crystals of [1](ClO$_4$)·CH$_3$CN·H$_2$O suitable for X-ray analysis.

[Ru(Me$_3$[9]aneN$_3$)(bpy)(NO)][ClO$_4$]$_3$, [2](ClO$_4$)$_3$. A total of 48 mg (0.084 mmol) of [Ru(Me$_3$[9]aneN$_3$)(bpy)(NO$_2$)]ClO$_4$ was dissolved in 5 mL of water. The solution was slowly acidified to pH 1 by dropwise addition of 1 M HClO$_4$ under constant stirring in an ice bath. Almost immediately the red solution turned yellowish. The reaction mixture was concentrated on a rotary evaporator to less than 5 mL; after adding 50 mg of NaClO$_4$ (0.41 mmol), it was left overnight at 4 °C to yield a yellow precipitate, which was collected by filtration and dried over silicagel. The crude product was recrystallized three times by slow evaporation from aqueous 0.1 M HClO$_4$, yielding 40 mg (63%) of yellow crystals already suitable for X-ray analysis. Anal. Calcd for [2](ClO$_4$)$_3$, C$_{19}$H$_{29}$N$_6$Cl$_3$O$_{13}$Ru (MW: 756.90 g mol$^{−1}$): C, 30.2; H, 3.9; N, 11.1. Found: C, 30.1; H, 4.1; N, 11.1. IR (KBr pellet): ν_{NO} = 1899 cm$^{−1}$. UV–vis: λ_{max}/nm (ε/M$^{−1}$ cm$^{−1}$), in H$_2$O: 492 (6.1 × 10^1), 340 (sh) (4.4 × 10^3), 312 (9.7 × 10^3), 256 (8.7 × 10^3); in CH$_3$CN: 460 (3.4 × 10^2), 338(sh) (4.7 × 10^3), 310 (9.1 × 10^3), 252 (8.9 × 10^3). ^{1}H NMR (CD$_3$CN, δ/ppm): 9.08 (dd, 2H, $J_{\alpha\beta}$ = 6 Hz, $J_{\alpha\gamma}$ = 1.1 Hz, H$_\alpha$), 8.79 (dd, 2H, $J_{\sigma\gamma}$ = 8.1 Hz, $J_{\sigma\beta}$ = 1.5 Hz, H$_\sigma$), 8.63 (ddd, 2H, $J_{\gamma\sigma}$ = 8.1 Hz, $J_{\gamma\beta}$ = 7.6 Hz, $J_{\gamma\alpha}$ = 1.1 Hz, H$_\gamma$), 8.16 (ddd, 2H, $J_{\beta\gamma}$ = 7.6 Hz, $J_{\beta\alpha}$ = 6 Hz, $J_{\beta\sigma}$ = 1.5 Hz, H$_\beta$), 3.86 (m, 2H, H$_{CH_2}$), 3.83 (m, 2H, H$_{CH_2}$), 3.76 (m, 2H, H$_{CH_2}$), 3.71 (m, 2H, H$_{CH_2}$), 3.62 (m, 2H, H$_{CH_2}$), 3.59 (s, 6H, H$_x$), 3.47 (m, 2H, H$_{CH_2}$), 2.12 (s, 3H, H$_y$); ^{13}C NMR (CD$_3$CN, δ/ppm): 156.25 (C$_\pi$), 153.06 (C$_\alpha$), 145.69 (C$_\gamma$), 131.43 (C$_\beta$), 128.14 (C$_\sigma$), 65.33 (CH$_2$), 63.70 (CH$_2$), 61.30 (CH$_2$), 57.07 (CH$_3$), 52.41 (CH$_3$).

[Ru(Me$_3$[9]aneN$_3$)(bpy)(^{15}NO)](ClO$_4$)$_3$, [^{15}2](ClO$_4$)$_3$. A total of 39 mg of [Ru((Me$_3$[9]aneN$_3$)(bpy)(OH$_2$)](ClO$_4$)$_2$ (0.060 mmol) and 145.4 mg of Na^{15}NO$_2$ (0.22 mmol) were suspended in 10 mL of water. The dark red mixture was refluxed for 1 h under Ar, yielding an orange solution. The reaction mixture was then acidified to pH 1 by dropwise addition of 1 M HClO$_4$ under constant stirring in an ice bath. Almost immediately the red solution turned yellowish. The reaction mixture was concentrated on a rotary evaporator to less than 5 mL, and after adding 64 mg of NaClO$_4$ (0.61 mmol) was left overnight at 4 °C to yield a yellow precipitate, which was collected by filtration and dried over silica gel. Yield: 33 mg (72%). The identity and purity of the product were corroborated by spectroscopic means (IR, UV−vis, and ^{1}H/^{13}C NMR). IR (KBr pellet): ν_{NO} = 1861 cm$^{−1}$.

Physical Determinations. Microanalytical data for C, H, and N were obtained with a Carlo Erba EA 1108 analyzer. UV−vis spectra were recorded with either an HP8453 or an HP8452A diode array spectrometer. IR spectral measurements were carried out with KBr pellets, using alternatively one of two FT spectrophotometers, a Nicolet 150P and a Thermo Nicolet AVATAR 320. The ^{1}H NMR spectra were measured with a 500 MHz Bruker AM 500 spectrometer; chemical shifts are referred to TMS. Cyclic voltammetry (CV) measurements in acetonitrile employing 0.1 M Bu$_4$NPF$_6$ as supporting electrolyte were performed with a standard three-electrode cell containing a working vitreous carbon electrode (3 mm Ⓓ), a Pt wire as a counterelectrode, and a silver wire plus an internal ferrocene (Fc) standard as a reference. In water we employed a similar arrangement except that the reference was a standard Ag/AgCl (3 M NaCl) commercial electrode (BAS). The potential of the working electrode was controlled with a TEQ-03 potentiostat. The spectroelectrochemical experiments in the UV−vis region were done

in a homemade cell containing a quartz cuvette (1 cm path). In all cases the ionic strength I was fixed to 1 M with NaCl in water or 0.1 M Bu$_4$NPF$_6$ in acetonitrile. The Ag/AgCl (3 M NaCl) and Ag/AgNO$_3$ (0.01 M) electrodes were used as a reference in aqueous solution and organic medium, respectively. The working electrode was a Pt net, and a Pt wire was the counterelectrode. The system was maintained at 25 ± 0.1 °C for the experiments in water and at −30 ± 1 °C for those in acetonitrile (RC6 LAUDA thermostat) and was entirely purged with Ar. Throughout this work, all the reported redox potentials are referred to Ag/AgCl, 3 M NaCl (0.21 V vs NHE). A typical spectroelectrochemical experiment required the application for a short period of time of a cathodic potential that induced charge circulation at the working electrode. Then the electrolysis was interrupted to allow the homogenization of the solution and simultaneous recording of the electronic spectrum and the open-circuit potential of the solution. The redox potentials and the disclosed UV−vis spectra of all the species present in solution were obtained by global analysis.[43] The procedure involved a simultaneous multiwavelength fitting, assuming that all the redox-active couples present in solution behave according to the Nernst equation.[44] pH-dependent experiments in water required different buffer solutions, depending on the pH. Because of the acid−base interconversion between [**1**]$^+$ and [**2**]$^{3+}$ in aqueous solution, the first reduction step of [**2**]$^{3+}$ was always performed at pH close to 2. The pH of the solution was subsequently adjusted to the desired value, employing appropriate buffer solutions (H$_2$PO$_4^-$/HPO$_4^{2-}$ or B(OH)$_4^-$/B(OH)$_3$). In the IR region, the spectroelectrochemistry was performed in an optically transparent thin layer electrode (OTTLE) cell described elsewhere.[45]

Kinetic studies for the addition of OH$^-$ to yield the corresponding nitro species were done under pseudo-first-order conditions, at I = 1 M (NaCl). Solutions at different [OH$^-$] were prepared by mixing 1 mL of a 6.31×10^{-5} M solution of [**2**]$^{3+}$ (0.01 M HCl, I = 1 M, NaCl) with 1 mL of the appropriate (H$_2$PO$_4^-$/HPO$_4^{2-}$ or B(OH)$_4^-$/B(OH)$_3$) buffer solution (0.33 M, I = 1 M, NaCl) in a 1 cm path length quartz cuvette. In all cases, the pH was checked after each kinetic run. The pseudo-first-order kinetic constants k_{obs} were obtained by multiwavelength global analysis, employing data measured in the UV−vis−NIR range. Plots of k_{obs} vs [OH$^-$] were employed to calculate the second-order rate constant (see text). Rate constants, k_{OH}, at different temperatures (range 20−40 °C) were employed to estimate the activation parameters (enthalpies and entropies) through an Eyring plot, $\ln(k_{OH}/T)$ vs $1/T$. The determination of the equilibrium constant for the addition of OH$^-$ was performed spectrophotometrically, employing equilibrated solutions containing [**1**]$^+$ and [**2**]$^{3+}$ at different pH values (H$_2$PO$_4^-$/HPO$_4^{2-}$ 0.33 M buffer solution, I = 1 M, NaCl). The solutions were allowed to equilibrate for 24 hs before recording the spectra, which were treated with global analysis techniques.[43,46]

X-ray Crystallographic Data Collection and Refinement of the Structures. Tiny, single crystals of red [**1**](ClO$_4$) and yellow [**2**](ClO$_4$)$_3$ were coated with perfluoropolyether, picked up with nylon loops, and mounted in the nitrogen cold stream of a Bruker AXS Kappa Mach3/APEX II diffractometer equipped with a Mo-target rotating-anode X-ray source and INCOATEC Helios Mirror X-ray optics (λ = 0.71073 Å). Final cell constants were obtained from least-squares fits of several thousand strong reflections. Intensities of redundant reflections were used to correct for absorption using the program SADABS.[47] The structure was readily solved by Patterson methods and subsequent difference Fourier techniques. The Siemens ShelXTL[48] software package was used for solution and artwork of the structures, and ShelXL97[49] was used for the refinement. All non-hydrogen atoms were anisotropically refined, and hydrogen atoms bound to carbon were placed at calculated positions and refined as riding atoms with isotropic displacement parameters. Hydrogen atoms bound to the water molecule in [**1**](ClO$_4$) could not be located from the difference map due to disorder.

All components in the unit cell of [**1**](ClO$_4$) reside on, or next to, a crystallographic mirror plane, which leads to severe disorder of the macrocyclic ligand in the cation, the anion, the acetonitrile, and the water molecule of crystallization. A split atom model with restrained

thermal displacement parameters and bond distances using EADP and SADI instructions of ShelXL97 was successfully refined to account for this disorder.

Several crystals of [**2**](ClO$_4$)$_3$ were mounted and tested on the diffractometer, but reflex profiles showed that most of them were twined. Intensity data were collected on the best specimen, but refinement of the structure showed that there must have been a tiny non meroheral twin component present in the crystal which gave rise to a number of reflections with increased intensities. This resulted in some unusually high final difference density peaks. The two most intense peaks show densities of about 4.7 and 3.7 e Å^{-3} (see level-B alarm in Checkcif file), and there are five more peaks with intensities between 2 and 1.5 e Å^{-3} which cannot be chemically interpreted.

Final crystallographic data and values of R_1 and wR of all crystals are listed in Table 1, while the main angles and distances are listed in Table 2.

Table 1. Crystallographic Data

	[**1**](ClO$_4$)·CH$_3$CN·H$_2$O	[**2**](ClO$_4$)$_3$
formula	C$_{21}$H$_{34}$ClN$_7$O$_7$Ru	C$_{19}$H$_{29}$Cl$_3$N$_6$O$_{13}$Ru
M$_r$	633.07	756.90
crystal system	orthorhombic	orthorhombic
space group	Pnma	Pbca
a/Å	25.250(9)	15.1877(19)
b/Å	12.053(4)	11.7191(15)
c/Å	8.325(3)	30.919(4)
V/Å^3	2533.60(15)	5503.20(12)
Z	4	8
D_{calc}/ Mg m^{-3}	1.660	1.827
T/K	100(2)	100(2)
μ, mm^{-1}	0.781	0.938
data/parameters	5296/382	9601/272
θ range/deg	3.38 −33.89	1.32 −32.07
collected/unique refl.	54996/5296	113531/9601
R_1, wR_2 ($I > 2\sigma(I)$)^a	0.0688, 0.1676	0.0608, 0.1433
R_1, wR_2 (all data)	0.0745, 0.1706	0.0783, 0.1529
GoF (F^2)	1.263	1.187

^{a}R-indices defined as: $R_1 = \Sigma||F_o| - |F_c||/\Sigma|F_o|$, $wR_2 = [\Sigma w(F_o^2 - F_c^2)^2/\Sigma w(F_o^2)^2]^{1/2}$.

Theoretical Calculations. We employed density functional theory (DFT) computations to fully optimize the ground-state geometries of all the species described in this work. The calculations were done with Gaussian 03[50] using Becke's three parameter hybrid functional with the correlation functional of Lee, Yang, and Parr formalized as the B3LYP hybrid functional[51] and the effective core potential basis set LanL2DZ,[52] which proved to be suitable for geometry predictions in coordination compounds containing metals of the second row of the transition elements in the Periodic Table. We used tight SCF convergence criteria and default settings in the geometry optimizations. For the species holding bent Ru−N−O moieties the computations involved a potential energy surface scan of the dihedral O−N−Ru−N(bpy) angle, which revealed in all cases two possible local minima corresponding roughly to a 180° change in the above-mentioned dihedral angle. The nature of the resulting stationary points was in all cases tested by computing the vibrational spectrum. The geometry of the two conformers obtained for each species turned out to be very similar, with practically identical coligand environments except for the disposition of the NO fragment. The explored potential energy surfaces were rather flat with small energy barriers between conformers compatible with free rotation of the NO moiety.

The analysis of the electronic structure was complemented with (TD)DFT computations including up to 70 states of the same multiplicity as that of the ground state. The spectra were computed at the gas-phase geometry of the lowest energy conformer of each species, and solvation effects in aqueous solution were taken into

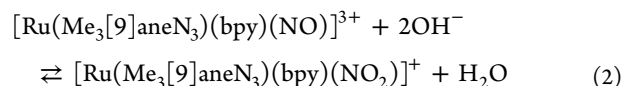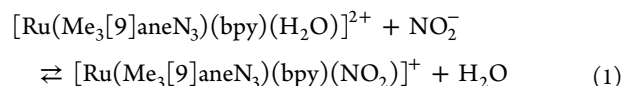**Table 2. Selected Bond Lengths (Å) and Angles (deg)**

	[1](ClO₄)·CH₃CN·H₂O	[2](ClO₄)₃
Ru1–N1	2.018(5)	1.768(4)
Ru1–N2	2.150(6)	2.128(4)
Ru1–N3	2.152(19)	2.142(3)
Ru1–N4	2.204(19)	2.150(3)
Ru1–N5	2.084(3)	2.143(3)
Ru1–N6	2.084(3)	2.129(3)
N1–O1	1.250(6)	1.135(5)
N1–O2	1.261(6)	–
N1–Ru1–N2	173.9(2)	171.30(15)
N1–Ru1–N3	92.6(3)	94.35(16)
N1–Ru1–N4	98.7(3)	88.85(15)
N1–Ru1–N5	87.20(13)	94.50(14)
N1–Ru1–N6	87.20(13)	93.84(16)
N2–Ru1–N3	82.1(4)	81.95(13)
N2–Ru1–N4	81.5(4)	82.84(13)
N2–Ru1–N5	92.1(2)	93.88(13)
N2–Ru1–N6	98.6(2)	90.29(13)
N3–Ru1–N4	80.6(2)	81.61(13)
N3–Ru1–N5	100.2(3)	99.61(13)
N3–Ru1–N6	178.1(3)	171.41(14)
N4–Ru1–N5	174.0(3)	176.32(13)
N4–Ru1–N6	101.3(3)	101.16(13)
N5–Ru1–N6	77.83(18)	77.13(13)
Ru1–N1–O1	123.0(4)	172.5(4)
Ru1–N1–O2	120.0(3)	–
O1–N1–O2	117.0(4)	–

account, employing the PCM approximation, as implemented in *Gaussian 03*.

■ RESULTS AND DISCUSSION

Preparation, Structural Characterization, and Vibrational Analysis. The properties of octahedral $\{MNO\}^n$ ($n = 6 - 8$) complexes may be tuned by an appropriate selection of the coordination sphere of the $\{MNO\}$ fragments. In general terms, octahedral $\{MNO\}^6$ species contain almost invariably quasi-linear MNO moieties, comparatively high ν_{NO} values ($1800-2000$ cm^{-1}), and are mostly unreactive toward nitrosyl dissociation. The reduced $\{MNO\}^{7,8}$ complexes display lower values of ν_{NO} and bent M–N-O moieties[2,4] and may experience labilization of NO or of the trans coligands.[53–56] The nature of the coordination sphere controls the redox potential of the $\{MNO\}$ fragments, so that electron-withdrawing ancillary ligands facilitate the accessibility of the lower oxidation states of the nitrosyl-group.[2] The overall composition of the coordination sphere also affects other properties, such as the electrophilic reactivity of $\{MNO\}^6$ species toward nucleophiles. The evidence shows that those species based on electron-acceptor coligands are more prone to react with nucleophiles such as OH$^-$,[57] a fact that may limit their use in aqueous medium. In order to obtain robust compounds with sufficiently high redox potentials and medium-to-low electrophilic reactivity to allow studying the different redox states in aqueous medium, we built the coordination sphere of a new system based on a mild σ-donor tridentate ligand, 1,4,7-trimethyl-1,4,7-triazacyclononane (Me₃[9]aneN₃), and 2,2′-bipyridine (bpy), a moderate acceptor bidentate fragment. The precursor [Ru(Me₃[9]aneN₃)(bpy)(H₂O)]²⁺ was readily obtained in good yield by a well-described procedure.[42] The

aqua complex was subsequently employed to prepare the nitro species following a traditional route that involves the direct reaction with NO₂$^-$ in aqueous medium (eq 1). The nitrosyl-compound became finally available upon acidification, due to the acid–base equilibrium described by eq 2.

$$[Ru(Me_3[9]aneN_3)(bpy)(H_2O)]^{2+} + NO_2^-$$
$$\rightleftharpoons [Ru(Me_3[9]aneN_3)(bpy)(NO_2)]^+ + H_2O \qquad (1)$$

$$[Ru(Me_3[9]aneN_3)(bpy)(NO)]^{3+} + 2OH^-$$
$$\rightleftharpoons [Ru(Me_3[9]aneN_3)(bpy)(NO_2)]^+ + H_2O \qquad (2)$$

Following these classic strategies we were able to isolate [**1**]⁺ and [**2**]³⁺ as ClO₄$^-$ salts (see Table 1). Figure 1 displays an ORTEP representation of the cations crystallized in this work. Table 2 lists the most relevant structural parameters. In both structures the metal atom is located in a distorted octahedral environment comprising six N-atoms. The nitro-species [**1**]⁺ displays a Ru–N(1) bond length of 2.018(5) Å, in agreement with other reports of Ru nitro complexes containing a bpy ligand.[58,59] The Ru–N(5) and Ru–N(6) distances of 2.084(3) Å and the Ru-bpy N(5)–Ru-N(6) bite angle of 77.83(18)° are also typical Ru-bpy metric parameters, and in fact compare well with the ones in the closely related [Ru(Me₃[9]aneN₃)bpy-(H₂O)]²⁺ (Ru–N(5) = 2.093(5) Å, Ru–N(6) = 2.087(4) Å, N(5)–Ru–N(6) = 77.6(2)°).[42] The three bond lengths to the tridentate Me₃[9]aneN₃ N atoms are slightly longer (Ru–N(2) = 2.150(6) Å, Ru–N(3) = 2.152 Å, and Ru–N(4) = 2.204 Å, and the three bite angles are slightly closer to 90° than in the case of the bpy, due to the higher flexibility of the Me₃[9]aneN₃ ring. Also in this case, the structural parameters are similar to the ones reported in the aqua species (Ru–N(2) = 2.087(4) Å, Ru–N(3) = 2.149(5) Å, and Ru–N(4) = 2.154(4) Å).[42]

The nitrosyl bearing cation [**2**]³⁺ shows an important contraction of the Ru–N(1) bond, which is at 1.768(4) Å. The N(1)–O(1) distance and the Ru–N–O angles are 1.135(5) Å and 172.5(4)°, respectively. The Ru–N(1) and N(1)–O(1) lengths are comparable to the ones reported in [Ru([9]aneS₃)bpy(NO)]³⁺ (1.766(4) Å and 1.127(5) Å, respectively),[60] [Ru(Tpb)bpy(NO)]²⁺ (1.753(3) Å and 1.138(3) Å),[59] and [Ru(Tpm)bpy(NO)]³⁺ (1.774(12) Å and 1.093 Å).[61] (Tpm = trispyrazolylmethane, Tpb$^-$ = hydro-trispyrazolylborate). The three Ru–N(Me₃[9]aneN₃) bonds are also shorter than those in [**1**]⁺ (2.128(4), 2.142(3) and 2.150(3) Å). These changes reflect the higher π-acceptor capability of the nitrosyl group (formally, a NO⁺-species) compared to the nitro-ligand, and are consistent with the ones observed in other $\{RuNO\}^6$ species. Strikingly, the nitro to nitrosyl conversion lengthens the Ru–N(5) and Ru–N(6) bonds to 2.143(3) and 2.129(3) Å, respectively, values which are much longer than in [**1**]⁺, in the structurally related [Ru(tpb)bpy(NO)]²⁺ (2.087(3) and 2.072(3) Å) and in [Ru(tpm)bpy(NO)]³⁺ (2.015(12) and 2.031(12) Å). This apparently inconsistent observation is actually due to enhanced steric interaction of the N(2)-methyl substituent with an aromatic ring of the bpy ligand. This interaction forces also a slight departure of the bpy from the plane defined by the metal center and the other equatorial nitrogen atoms. The overall metric parameters are consistent with the expectations according to the Enemark–Feltham model for a $\{Ru-NO\}^6$ formulation.[16] The comparison with the nitrosyl species based
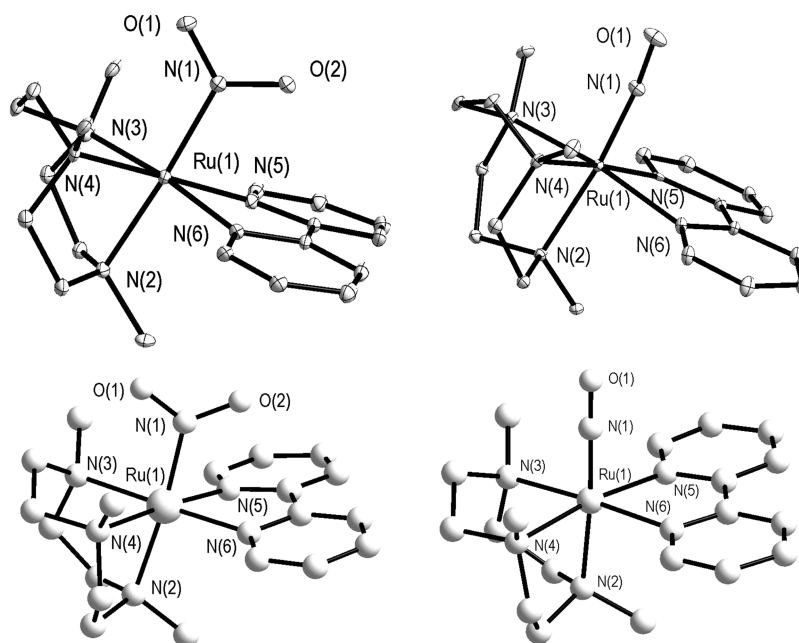
Figure 1. Structures of the cations in crystals of [1](ClO₄)·CH₃CN·H₂O (top, left) and [2](ClO₄)₃ (top, right). Perspective view with thermal ellipsoids at the 30% probability level. DFT optimized geometries for the isolated cations [1]⁺ (bottom, left) and [2]³⁺ (bottom, right) in vacuo.

Table 3. Selected Metric Parameters and Mayer Bond Orders (in parentheses) Obtained From DFT Computations

	[1]⁺	[2]³⁺	[2]²⁺	[2-H]²⁺	[2]⁺
Bond Lengths (Å)					
Ru1−N1	2.05 (0.48)	1.78 (1.04)	1.90 (0.84)	1.93 (0.77)	1.91 (1.18)
Ru1−N2	2.23 (0.31)	2.18 (0.54)	2.22 (0.39)	2.22 (0.37)	2.41 (0.20)
Ru1−N3	2.24 (0.37)	2.23 (0.53)	2.22 (0.41)	2.24 (0.44)	2.28 (0.32)
Ru1−N4	2.24 (0.35)	2.22 (0.52)	2.22 (0.42)	2.23 (0.43)	2.27 (0.32)
Ru1−N5	2.11 (0.39)	2.16 (0.50)	2.15 .(0.41)	2.14 (0.40)	2.10 (0.41)
Ru1−N6	2.13 (0.39)	2.18 (0.50)	2.15 (0.41)	2.15 (0.40)	2.11 (0.41)
N1−O1	1.30 (1.39)	1.18 (1.82)	1.22 (1.58)	1.28 (1.43)	1.27 (1.45)
N1−O2	1.29 (1.34)	−			
N1−H				1.05 (0.79)	
Bond Angles (deg)					
Ru1−N1−O1	120.3	179.5	142.4	127.5	122.9
Ru−N1−O2	120.6				

on Tpm and Tpb⁻ suggests a strong similarity in the donor/acceptor averaged properties of the coligand environments.

Table 3 and Figure 1 contain analogous information extracted from the DFT optimized geometries for [1]⁺ and [2]³⁺. The almost linear {RuNO} moieties observed in [2]³⁺ are properly described, as well as the structural changes expected in the nitrosyl-nitro acid−base conversion. A thorough comparison reveals that the theoretical Ru−N bond lengths are slightly (and consistently) overestimated, a behavior already reported when comparing experimental and theoretically produced bond lengths at this level of theory in transition metal complexes[62] and in particular in other {RuNO}⁶ systems.[57,61,63,64]

The DFT computations reproduce the principal features observed in the vibrational spectra of all the species and allow for a complete assignment of the vibrational modes.[65] In general terms, there is a very good agreement between experimental and theoretically derived magnitudes, a fact that contributes to validation of the theoretical methodology. The computed ν_{NO} frequency for [2]³⁺, 1859 cm⁻¹, can be compared with 2219 cm⁻¹, obtained at exactly the same level

of theory for the free NO⁺ cation (Supporting Information, Table S2). Upon coordination the predicted ν_{NO} is reduced by ∼14%, an indication of π-backbonding, which involves partial population of a nitrosyl-centered antibonding orbital. The same comparison performed with [Fe(NO)(cyclam-ac)]²⁺ (cyclam-ac⁻ = 1,4,8,11-tetraazacyclotetradecane-1-acetate) led to a 20% reduction of ν_{NO},[66] suggesting that the backbonding in the ruthenium complex is smaller than in the iron case. A similar behavior was observed in the backbonding trends in the series of [Mᴵᴵ(CN)₅pz]³⁻ complexes (M = Fe, Ru, Os)[67] and interpreted in terms of the more favorable energy match between d_{Fe} and π^*_{pz} orbitals over the lesser overlapping capability of the 3d orbitals.

The experimental value of 1899 cm⁻¹ for ν_{NO} is intermediate in the context of the wide range (∼1800−2000 cm⁻¹) measured for nitrosyl-complexes with a formally assigned NO⁺-character (see Table 4). Complexes with higher values of ν_{NO} contain strongly π-acceptor coligands that compete with nitrosyl for the electron density.[2,57] On the other hand, the combination of donor- and acceptor-coligands in the coordination sphere of [2]³⁺ makes ruthenium more electron-

Table 4. Selected Structural Parameters in Related Octahedral {MNO}^{n} Compounds (n = 6−8)

| compd	$d_{M-N}{}^a$	$d_{N-O}{}^a$	$\angle_{M-N-O}{}^b$	$\nu_{NO}{}^c$	ref
n = 6					
[Ru(Me$_3$[9]aneN$_3$)(bpy)(NO)](ClO$_4$)$_3$	1.768(4)	1.135(5)	172.5(4)	1899	this work
[Ru(Me$_3$[9]aneS$_3$)(bpy)(NO)](ClO$_4$)$_3$	1.766(4)	1.127(5)	176.5(4)	1945	60
[Ru(OEP)(NO)(OH$_2$)]BF$_4$·H$_2$O	1.888(5)	1.138(12)	171.0(7)	1853	68
Ru(TTP)(NO)(OH)	1.751(5)	1.142(8)	167.4(6)	1813	69
Ru(OEP)(NO)(ONO)	1.758(7)	1.177(9)	174.0(8)	1835	70
Ru(OEP)(NO)(S-NACysMe)	1.790(5)	1.123(8)	174.8(6)	1791	71
Ru(OEP)(NO)(p-C$_6$H$_4$F)	1.807(3)	1.146(4)	154.9(3)	1759	72
[Ru(NH$_3$)$_5$(NO)]Cl$_3$·H$_2$O	1.770(9)	1.172(4)	172.8(9)	1903	4, 73
t-[Ru(NH$_3$)$_4$(NO)(OH$_2$)]Cl$_3$·H$_2$O	1.793, 1.715(5)	1.142(7)	178.1(5)	1912	74
[Ru(cyclam)Cl(NO)](ClO$_4$)$_2$	1.747(4)	1.128(5)	–	1875	56, 75
[Ru(bpy)$_2$Cl(NO)](ClO$_4$)$_2$	1.751(6)	1.132(9)	170.4(5)	1920	76
[Ru(DMAP)$_4$(OH)(NO)](BF$_4$)$_2$·2H$_2$O	1.748(8)	1.245(8)	169.3(6)	1832	64
Na$_2$[Ru(CN)$_5$NO]·2H$_2$O	1.773(3)	1.130(4)	174.4(3)	1926	77
[Fe(cyclam-Ac)(NO)](ClO$_4$)Cl·H$_2$O	1.663(4)	1.132(5)	175.5(3)	1893	66
[Fe(TPP)(NO)(OH$_2$)]ClO$_4$	1.652(5)	1.15(0)	174.4(10)	1937	72
[Fe(OEP)(NO)(1-MeIm)]ClO$_4$	1.6465(17)	1.135(2)	177.28(17)	1921	78
Fe(TpivPP)(NO)(NO$_2$)	1.668(2)	1.132(3)	180.0	1893	79
Fe(OEP)(NO)(p-C$_6$H$_4$F)	1.728(2)	1.153(3)	157.4(2)	1839	80
[Fe([9]aneN$_3$)(NO)(ONO)(NO$_2$)]ClO$_4$	1.644(4)	–	171.2(4)	1907	81
[Fe(pyS$_4$)(NO)]PF$_6$	1.634(3)	1.141(3)	179.5(3)	1893	82
n = 7					
[Fe(Me$_3$[9]aneN$_3$)(NO)](N$_3$)$_2$	1.738(5)	1.142(7)	155.5(10)	1690	83
t-[Fe(cyclam)Cl(NO)]ClO$_4$	1.820(4)		144.0(6)	1611	81
Fe(pyS$_4$)(NO)·2CH$_2$Cl$_2$	1.712(3)	1.211(7)	143.8(5)	1648	82
[Fe(NO)(pyN$_4$)]Br$_2$	1.737(6)	1.175(8)	139.4(5)	1620	84
[Fe(cyclam-Ac)(NO)](PF$_6$)$_2$	1.722(4)	1.166(6)	148.7(4)	1615	66
n = 8					
[Rh(AcN)$_3$(NO)(PPh$_3$)$_2$](PF$_6$)$_2$	2.026(8)	1.139(10)	118.4(6)		22
[Ir(AcN)$_3$(NO)(PPh$_3$)$_2$](PF$_6$)$_2$	1.965(20)	1.28(2)	111(1)	1685	21
[Pd(CH$_2$CMe$_2$-o-C$_6$H$_4$)(tpb)(NO)]	2.016(5)	1.151(7)	118.3(5)	1650	20
t-[CoCl(NO)(en)$_2$](ClO$_4$)	1.820(11)	1.043(17)	124.4(11)		24
[Pt(NH$_3$)$_4$(SO$_4$)(NO)](HSO$_4$)·CH$_3$CN	2.081(2)	1.133(3)	117.4(2)	1714	35
[Co(NO)(das)$_2$(NCS)](NCS)	1.85(1)	1.00(1)	132.3(14)	1587, 1561	23
[Co(NH$_3$)$_5$(NO)]Cl$_2$	1.871(6)	1.154(7)	119.0(9)		34
IrHCl$_2$(PPh$_3$)$_2$(HNO)	1.879(7)	1.235(11)	129.8(7)	1493	30
OsCl$_2$(CO)(PPh$_3$)$_2$(HNO)	1.915(6)	1.193(7)	136.9(6)	1410	29
Ru(pyS$_4$)(HNO)	1.875(7)	1.242(9)	130.0(6)	1358	31

^{a}Distances in Å. ^{b}In degrees. ^{c}Infrared frequencies in cm^{-1}. Abbreviations used for the ligands: [9]aneN$_3$ = 1,4,7-triazacyclononane; Me$_3$[9]aneN$_3$ = 1,4,7-trimethyl-1,4,7-triazacyclononane; bpy =2,2′-bipyridine; Me$_3$[9]aneS$_3$ = 1,4,7-trimethyl-1,4,7-trithiocyclononane; OEP = octaethylporphyrin dianion; TTP = tetra-p-tolylporphyrinato dianion, NACysMe = N-acetyl-L-cysteinate methyl ester; TPP = meso-tetraphenylporphyrin dianion; 1-MeIm = 1-methylimidazole; cyclam =1,4,8,11-tetraazacyclotetradecane; cyclam-Ac = 1,4,8,11-tetraazacyclote-tradecane-1-acetate; TpivPP = α,α,α,α, -tetrakis(o-pivalamidophenyl)-porphyrin dianion; pyS$_4$ = 2,6-bis-(2-mercaptophenylthiomethyl)pyridine dianion; pyN$_4$ = N,N′-bis(2-pyridylmethyl)-N-bis(2-pyridyl)methylamine; AcN = acetonitrile; PPh$_3$ = triphenylphosphine; tpb = hydro-trispirazolylborate; en =1,2-diaminoethane; das = o-phenylenebis(dimethylarsine)

rich and a stronger π-donor toward nitrosyl. The downward shift in ν_{NO} to 1861 cm^{-1} with labeled ^{15}N agrees with values found for other nitrosyl-complexes.[59,64,66]

{RuNO}^{6} Species in Aqueous Solution. Solutions of the nitro-complex [**1**]$^+$ are intensely red colored. Figure 2 shows the electronic spectrum of [**1**]$^+$ in water at pH 10.0 overlaid with the (TD)DFT computed transitions and a MO diagram obtained from the DFT computations, which help to establish the electronic structure for the species. A complete list of the computed transition energies, intensities and orbital description as obtained from (TD)DFT can be found in the Supporting Information (Tables S4−S6). Table 6 lists the experimental energies and intensities. The MO diagram obtained from the DFT computations (Figure 2) helps in the following discussion of the spectrum. The degeneracy of the t$_{2g}$ set is completely

lifted because of the low symmetry of the molecule, yielding three d orbitals of different (but close) energy. The LUMO of the molecule resides on a bpy-centered π* orbital. The latter is the acceptor orbital involved in the lowest energy metal-to-ligand charge transfer (MLCT) transition responsible for the lowest energy band of the spectrum. A second MLCT involving higher energy bpy orbitals shows up at lower wavelength, overlapped with the Ru−π*$_{NO2}$ CT absorption. A series of intraligand $\pi \rightarrow \pi$* transitions are responsible for the bands that show up at ∼300 nm.
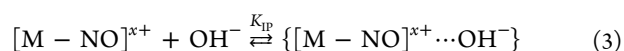
Figure 2 also displays the analogous information for [**2**]$^{3+}$. In this case the spectrum was recorded in acidic medium (pH 2.0). The most remarkable feature is the absence of the Ru $\rightarrow$ π*(bpy) MLCT bands in the visible region. This is a consequence of the strong π-interaction between metal d
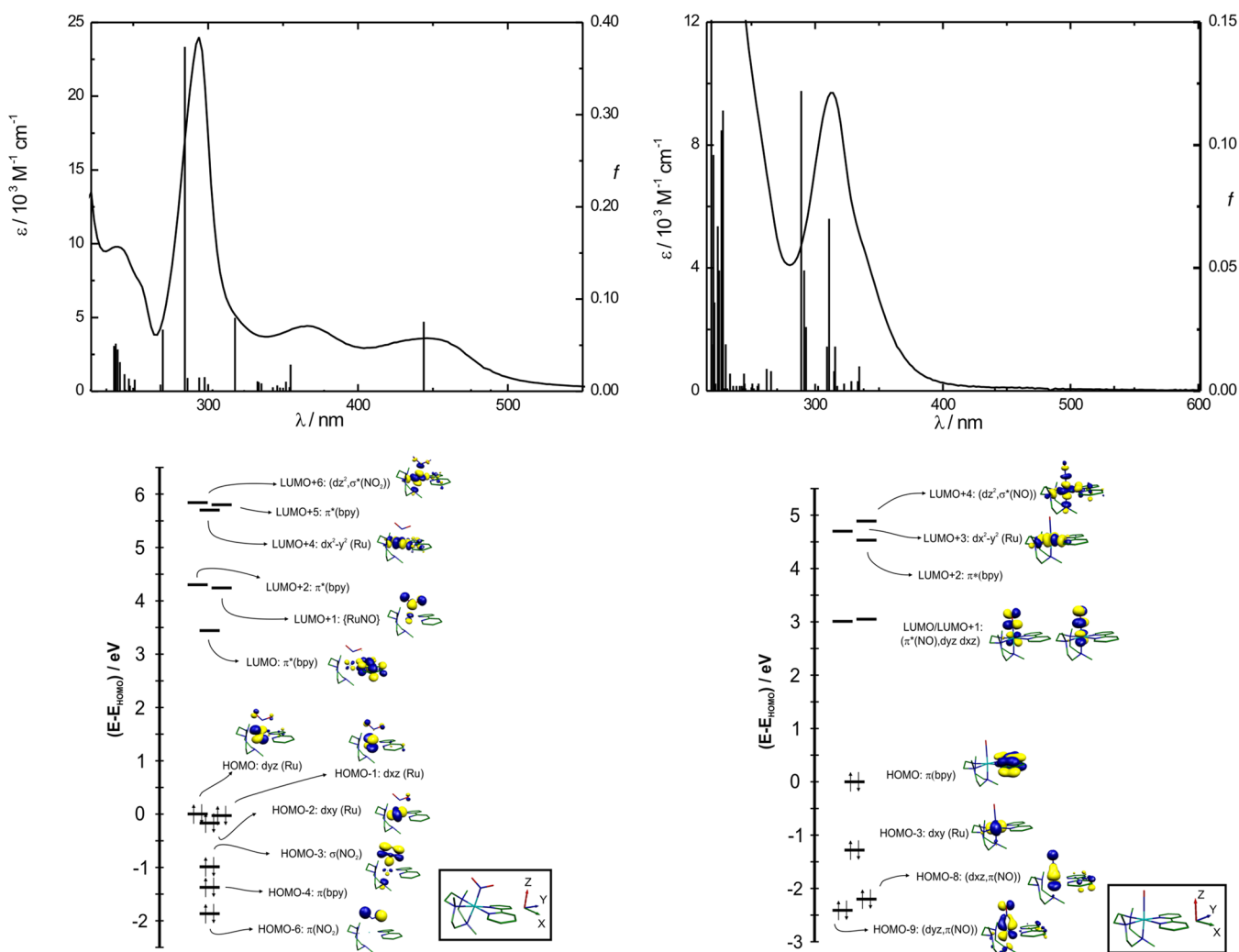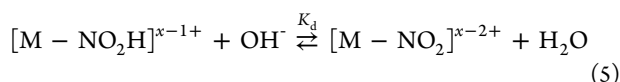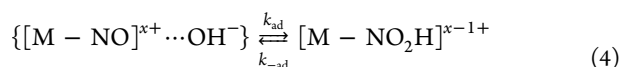
Figure 2. Experimental and computed ((TD)DFT) UV−vis spectrum and frontier orbitals of $[1]^+$ (left) and $[2]^{3+}$ (right) in water.

orbitals and π^*_{NO}-centered orbitals, which results in a large stabilization of the t_{2g} set. This phenomenon is common to other nitrosyl bearing species[61,63,64,85,86] and can be well appreciated in the molecular orbital diagram. The LUMO and LUMO+1 MOs are mostly located on the nitrosyl moiety with ∼27% contribution from metal center orbitals, reflecting a substantial π-backbonding comparable to the one calculated in $[Ru(tpm)(bpy)NO]^{3+}$ (25−30%)[61] and $[Ru(DMAP)_4(OH)-(NO)]^{2+}$ (30%).[64] This back-donation mechanism partially transfers electron density form the metal center to the π^* orbitals of the coordinated NO^+,[15] and is responsible for the observed lowering of ν_{NO} from 2377 cm^{-1} in free NO^+ [3] to 1899 cm^{-1} in $[2]^{3+}$. The light-yellow color of the aqueous solutions of $[2]^{3+}$ is mostly due to the low energy tail of intraligand- and ligand-to-ligand transitions. On the basis of the (TD)DFT analysis, the very weak absorption on the low energy side of the spectrum at ∼450−500 nm can be assigned to a $d_{Ru} \rightarrow \pi^*_{NO}$ CT transition. This interpretation agrees with reports for other octahedral $\{RuNO\}^6$ compounds.[54,63,86] The spectrum of $[2]^{3+}$ is virtually solvent independent (Supporting Information, Figure S6). On the contrary, the MLCT bands of the nitro-species $[1]^+$ shift to higher energy when the spectrum is recorded in water. This fact seems to be related to specific hydrogen-bond interactions between the NO_2^- groups and the solvent, as already described in other systems.[58]

Pseudo-octahedral nitrosyl species as the one described here are well-known for their inertness toward dissociation of the ligands in the coordination sphere. In contrast, they participate in electrophilic reactions that involve the (formally) coordinated NO^+. Apart from the inherent interest of this kind of processes, the conversion between coordinated NO_2^- and NO^+ is crucial at the early stages of nitrite-reductases activity, not only requiring N-bound nitrite coordination on a Fe(II)-aqua site, but also a proton-assisted dehydration leading to bound NO^+, which has an appropriate low-energy LUMO for further reduction.[10,87] Studying the reactions with aqueous OH^- is indispensable to establish the pH window where the nitrosyl species predominates over the nitro-complexes in the interconversion process described by eq 2. The reaction between $[2]^{3+}$ and OH^- is of first order in the concentration of the nitrosyl-bearing species. Experiments with different concentrations of the nucleophile (Supporting Information, Figure S7) rendered values for the first order (OH^-)-dependent rate constant k_{obs}. The mechanism[88] for the $NO^+ \rightarrow NO_2^-$ conversion (described by eq 2) involves several steps (eqs 3-5).

$$[M-NO]^{x+} + OH^- \underset{\rightleftarrows}{\overset{K_{IP}}{}} \{[M-NO]^{x+}\cdots OH^-\} \qquad (3)$$

$$\{[M - NO]^{x+} \cdots OH^-\} \underset{k_{-ad}}{\overset{k_{ad}}{\rightleftharpoons}} [M - NO_2H]^{x-1+} \qquad (4)$$

$$[M - NO_2H]^{x-1+} + OH^- \overset{K_d}{\rightleftharpoons} [M - NO_2]^{x-2+} + H_2O \qquad (5)$$

yielding the following rate law

$$\nu = k_{OH}\left\{[OH^-] + \frac{1}{[OH^-]K_{eq}}\right\}[[M - NO^{x+}]^-] \qquad (6)$$

where $K_{eq} = K_{IP}((k_{ad})/(k_{-ad}))k_d$ and $k_{OH} = K_{IP}k_{ad}$

At sufficiently high concentration of OH^-, eq 6 simplifies to

$$\nu = k_{OH}[OH^-][[M - NO]^{x+}] \qquad (7)$$

k_{OH} at 25.0 °C was extracted from the linear region of the k_{obs} vs $[OH^-]$ plot (Supporting Information, Figure S7) resulting in a value of $(1.266 \pm 0.007) \times 10^4 \ M^{-1} \ s^{-1}$. The K_{IP} value was estimated as 2.10 in terms of the Fuoss model,[89] employing the molecular volume obtained from the DFT computations to estimate the contact distance within the ion-pair. On this basis, k_{ad}, the intrinsic first-order rate constant associated with eq 4 results $(6.028 \pm 0.003) \times 10^3 \ s^{-1}$. The temperature dependence experiments allowed obtaining the activation parameters, $\Delta H^{\ddagger} = 20.2 \pm 0.1 \ kJ \ mol^{-1}$ and $\Delta S^{\ddagger} = +106.9 \pm 0.4 \ J \ K^{-1} \ mol^{-1}$, which agree with the general mechanistic picture of the addition reactions on bound nitrosyl.[57] The overall equilibrium constant K_{eq} obtained upon equilibration at different pH values resulted $(1.8 \pm 0.4) \times 10^{16}$. The most oxidizing nitrosonium-complexes afford larger equilibrium constants and nucleophilic addition rates, and in fact, $\ln (k_{ad})$ and the redox potential of the $\{MNO\}^6/\{MNO\}^7$ couple are linked by a linear free energy relation,[57] as frequently found in the correlation of kinetic vs thermodynamic parameters for a set of reactions governed by the same mechanism.[90] The newly reported compound fits well in the general trend observed for other nitrosyl-species (see later for the $E°$ value associated with the first reduction process). These experiments establish the pH regions of predominance and coexistence of $[1]^+$ and $[2]^{3+}$ and therefore the conditions required to safely use solutions of $[1]^+$, a piece of information that will become crucial when exploring the spectroscopic and redox properties of this species.

Redox Behavior, Accessibility and Characterization of the $\{RuNO\}^7$ State. Figure 3 shows a typical cyclic voltammogram (CV) of $[2]^{3+}$ in water solution (pH = 4.5, acetic acid/acetate 0.3 M buffer solution, I = 1M, NaCl). Within the redox window of the solvent, the species displays two 1-electron redox processes. The first wave at 0.20 V is reversible, as shown by ΔE_p in the range $60 - 90$ mV and $I_p \approx \nu^{1/2}$.[91] A similar reversible redox process is also observed in acetonitrile/0.1 M TBAPF$_6$ (Figure 3, bottom), though the half-wave potential is shifted to 0.53 V. We observed a shift of the same sign but somewhat smaller magnitude (0.20 V) for the same process in cis-$[Ru(L^{py})NO]^{3+}$ (L^{py} = N-(2-methylpyridyl)1,4,8,11-tetraazacyclotetradecane)[86] and an almost identical difference of about 300 mV in $[Ru(tpm)(bpy)-NO]^{3+}$.[61] The differences can be traced back to changes in the dielectric properties of both solvents, which would favor the reduction process in a less polar medium.

Figure 4 shows the spectral evolution for the electrochemical reduction of $[2]^{3+}$ in water monitored in the UV−vis range (see details in the Experimental Section). The redox conversion proved fully reversible, and solutions of the reduced species
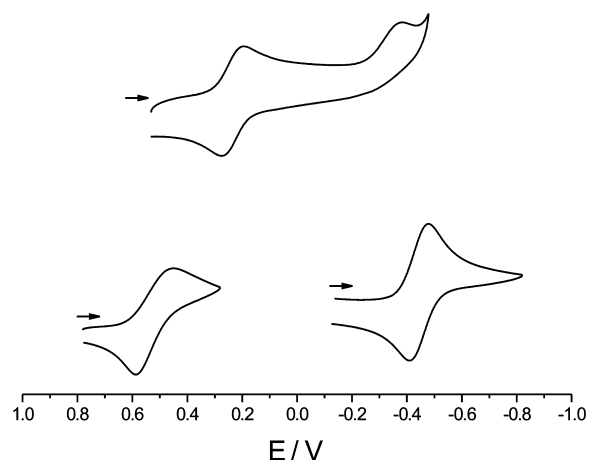
Figure 3. Cyclic voltammogram of $[2]^{3+}$ in water, at pH 4.5 (acetic acid/acetate 0.3 M, I = 1 M (NaCl), (top) and in acetonitrile, I = 1 M (TBAPF$_6$) (bottom), Scan rate = 200 mV s^{-1}, T = 25 °C. E in V vs AgCl (NaCl 3M)/Ag^0.
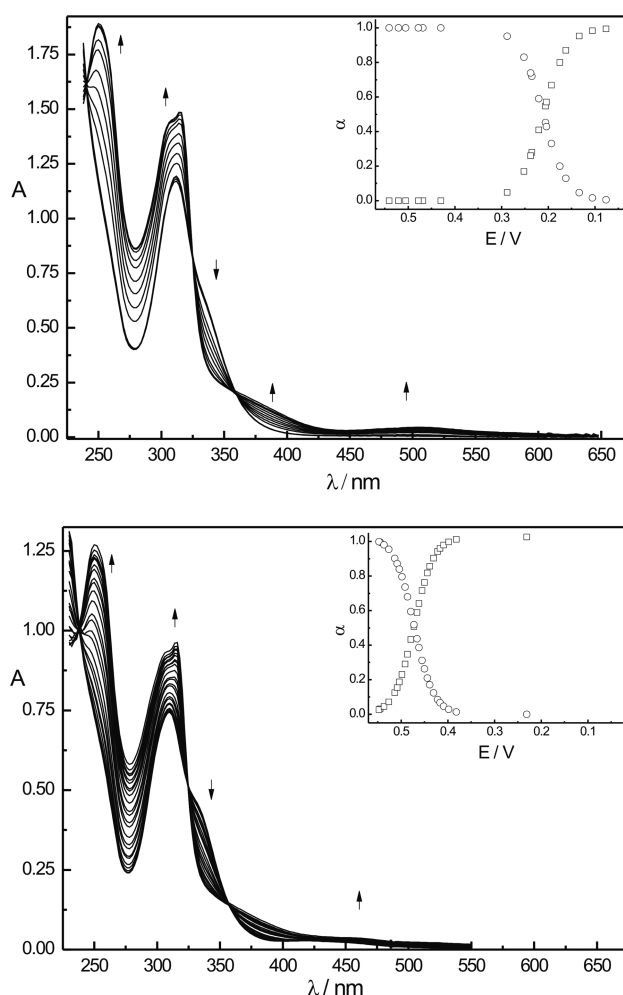
Figure 4. Spectroelectrochemistry of the $[2]^{3+} \rightarrow [2]^{2+}$ redox conversion in aqueous HCl, pH = 2.0, I = 1 M (NaCl) (top), and in acetonitrile, I = 1 M (TBAPF$_6$), T = −30 °C (bottom). See the Experimental Section for details. The arrows indicate the spectral changes along the reduction process. The insets represent the fraction of $[2]^{3+}$ and $[2]^{2+}$ as obtained from the global analysis.

Table 5. IR Vibrational Frequencies and Redox Potentials for $[Ru(Me_3[9]aneN_3)(bpy)(NO)](ClO_4)_3$ and Selected Nitrosyl Species

compd	$\nu_{NO}{}^a$	$E_{1/2}{}^b$		ref
		H₂O	AcN	
$[Ru(Me_3[9]aneN_3)(bpy)(NO)](ClO_4)_3$	1899^c $(1861)^d$	0.20^f $(0.21)^h$	0.53^f $(0.47)^i$	this work
	1934^e $(1898)^{d,e}$	-0.56^f $(-0.56)^h$	-0.44^f $(-0.56)^i$	
		$0.01^{f,g}$ $(0.02)^{g,h}$		
$[Ru(Tpm)(bpy)(NO)](ClO_4)_3 \cdot 1/2H_2O$	1959^c	0.31	0.60	61
	1962^e		-0.20	
$[Ru(cyclam\text{-}py)(NO)](PF_6)_3$	1917^c	-0.02	0.18	86
			-0.75^j	
$[Ru(DMAP)_4(OH)(NO)](BF_4)_2 \cdot 2H_2O$	1832^c		-0.46	64
	1844^e		-1.29	
$[Ru(bpy)_2(Cl)(NO)](PF_6)_2$	1912^c		0.23	57, 76, 92
			-0.39^j	
$[Ru(trpy)(bpy)(NO)](PF_6)_3$	1952^c		0.48	93
			-0.17^j	
$[Ru(py)_4(Cl)(NO)](PF_6)_2 \cdot 1/2H_2O$	1910^c		0.34	57, 76, 92
			-0.56^j	
$[Ru(Me_3[9]aneS_3)(bpy)(NO)](ClO_4)_3$	1945^c		0.52	60
			0.10^j	
$[Fe(cyclam\text{-}Ac)(NO)](ClO_4)Cl \cdot H_2O$	1893^c		0.49	66
	1903^e		-0.89	

^{a}cm^{-1}. $^b E_{1/2}$ values in V vs Ag/AgCl (3 M, NaCl) obtained from CV experiments, unless otherwise stated. ^{c}In KBr. $^d[Ru(Me_3[9]aneN_3)(bpy)(^{15}NO)](ClO_4)_3$. ^{e}In acetonitrile/0.1 M (n-Bu)$_4$NPF$_6$. ^{f}Obtained from CV or SWV scans. See text for details. ^{g}Extrapolated to pH = 0. ^{h}From spectroelectrochemistry at room temperature. See text for details. ^{i}From spectroelectrochemistry at -40 °C. See text for details. ^{j}Irreversible E_{pc}. Abbreviations used for the ligands: Me$_3$[9]aneN$_3$ = 1,4,7-trimethyl-1,4,7-triazacyclononane; bpy =2,2′-bipyridine; Me$_3$[9]aneS$_3$ = 1,4,7-trimethyl-1,4,7-trithiocyclononane; DMAP = 4-dimethylaminopyridine; cyclam-Ac = 1,4,8,11-tetraazacyclotetradecane-1-acetate; Tpm = tris-pyrazolyl methane; trpy =2,2′:6′,2″-terpyridine; cyclam-py = N-(2-methylpyridyl) 1,4,8,11-tetraazacyclotetradecane; py = pyridine.

remained stable for several hours in the absence of oxygen. A global analysis performed over the spectroscopic data is consistent with the presence of only two colored species along the whole electrochemical conversion. The quantitative treatment of the data nicely confirms the clean 1-electron reduction yielding the reduced $[2]^{2+}$, anticipated by the CV experiment. The global analysis also renders the UV−vis spectra of the pure species and the redox potential, which agrees within error of the methodology with data obtained by CV (Table 5). The absorption spectrum of $[2]^{2+}$ is displayed in Figure 5, and the absorption maxima and extinction coefficients are summarized in Table 6. It is worth noting that the absorption spectrum of solutions of $[2]^{2+}$ remains unchanged for long periods of time even if after the controlled potential reduction of $[2]^{3+}$ the pH of the solutions is modified appropriately to any value in the range between 1 and 14. As we will see later, these solutions will allow exploring the redox behavior of $[2]^{2+}$ in a wide range of acidity conditions.

Spectral changes in the UV−vis region observed upon reduction of $[2]^{3+}$ in acetonitrile were almost identical to the ones observed in water (Table 6), suggesting that the identity and the electronic structures of the 1-electron reduced species in water and acetonitrile are the same. In addition, the use of acetonitrile as solvent enabled the possibility to explore the changes in the vibrational spectrum along the reduction process. In solution, $[2]^{3+}$ shows an intense peak associated to the NO stretching vibration at 1934 cm^{-1}, which shifts to 1898 cm^{-1} in the ^{15}N labeled analog $[^{15}2]^{3+}$. Upon 1-electron reduction, these bands shift to 1637 and 1605 cm^{-1}, respectively (see Figure 6). Nitrosyl-centered 1-electron reductions of octahedral {MNO}^{6} species, as already reported for M = Fe and Ru,^{2,66} are expected to induce a shift of ≈300

cm^{-1} in ν_{NO} along with significant structural changes along the M−N−O axis. The DFT geometry optimization of $[2]^{2+}$ (Figure 7a and Table 3) confirms this expectation. The computed values of ν_{NO} at 1620 and 1590 cm^{-1} for $[2]^{2+}$ and $[^{15}2]^{2+}$, respectively, are in very good agreement with the experiments. Altogether, UV−vis and IR spectroscopic results are compatible with the following stoichiometry of the redox process:

$$[Ru(Me_3[9]aneN_3)(bpy)(NO)]^{3+} + e^-$$
$$\rightarrow [Ru(Me_3[9]aneN_3)(bpy)(NO)]^{2+} \qquad (8)$$
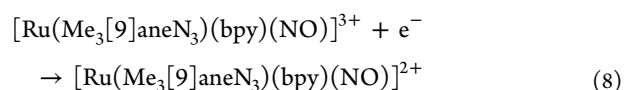
The DFT optimized structure of the $[2]^{2+}$ cation (Table 3 and Figure 7) reveals a marked lengthening of the Ru(1)−N(1) and N(1)−O(1) bonds to 1.90 and 1.22 Å, respectively, compared to $[2]^{3+}$, and the bending of the Ru−N(1)-O(1) angle to about 144°. The Ru−N(2) bond length (i.e., the one that involves the nitrogen atom trans to the NO group) increases by ∼0.04 Å. This fact reduces the steric interaction with the bpy-atoms and allows for a slight shortening of the Ru−N(5) and Ru−N(6) bonds (Table 3). The structural changes combined with the reduction of the N(1)−O(1) Mayer bond order from 1.82 in $[2]^{3+}$ to 1.58 reflect the population of a formally π-antibonding orbital located mostly on the NO fragment. The computed spin density indicates that the SOMO is mostly π*$_{NO}$ in character (Supporting Information, Figure S8), in total agreement with a {RuNO}^{6} → {RuNO}^{7} conversion. This fact is also compatible with the 9% reduction of ν_{NO} if compared to the one obtained for NO in the gas phase (1771 cm^{-1}, Supporting Information, Table S2). MO analyses reveal a split t$_{2g}$ set closer in energy to the HOMO of the molecule than in the nitrosyl parent compounds,
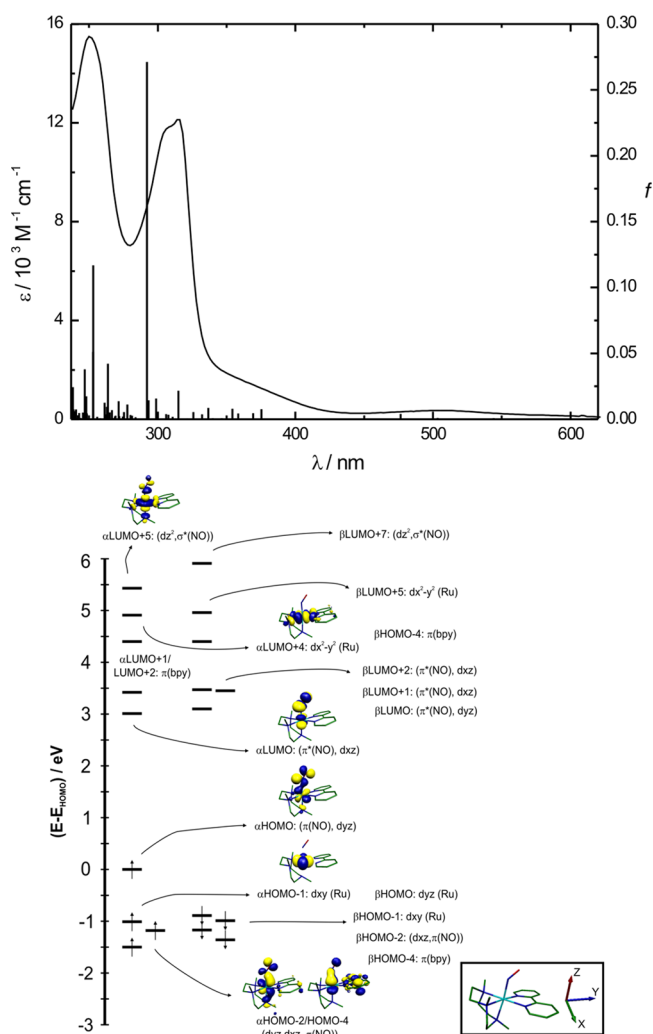
Figure 5. Experimental and (TD)DFT computed spectrum in water, and MO diagram of [2]²⁺.

Table 6. Electronic Spectra of [1]⁺, [2]³⁺, [2]²⁺, [2]⁺, and [2-H]²⁺

	λ_{max}, nm (ε, M⁻¹ cm⁻¹)	
	H₂O	CH₃CN
[1]⁺	294 (2.40 × 10⁴)	295 (2.59 × 10⁴)
	366 (4.43 × 10³)	338 (5.96 × 10³)
	446 (3.59 × 10³)	480 (5.29 × 10³)
[2]³⁺	312 (9.70 × 10³)	310 (9.06 × 10³)
	340sh (4.38 × 10³)	338sh (4.72 × 10³)
	492 (6.10 × 10¹)	460 (3.36 × 10²)
[2]²⁺	250 (1.55 × 10⁴)	252 (1.27 × 10⁴)
	316 (1.21 × 10⁴)	316 (1.05 × 10⁴)
	506 (3.55 × 10²)	506 (2.21 × 10²)
[2]⁺	290 (1.37 × 10⁴)	298 (1.82 × 10⁴)
	374 (2.02 × 10⁴)	356 (3.06 × 10³)
	440 (2.07 × 10²)	480 (3.56 × 10³)
[2-H]²⁺	258 (1.41 × 10⁴)	
	302 (1.14 × 10⁴)	
	318 (1.14 × 10⁴)	
	376 (5.67 × 10³)	

and a smaller π-interaction with the NO fragment, in agreement with a smaller reduction of the N–O stretching frequency
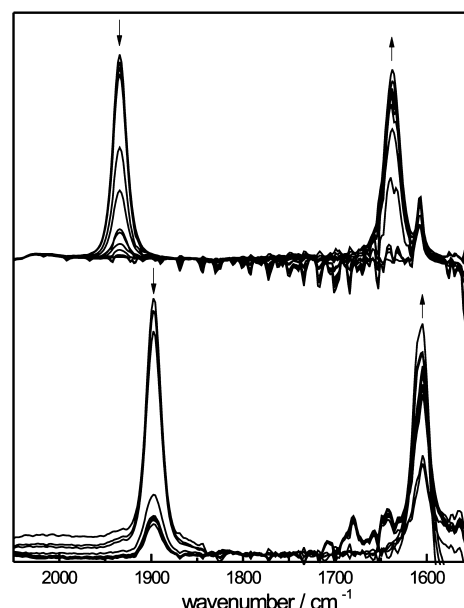

Figure 6. Spectroelectrochemistry of the [2]³⁺ → [2]²⁺ (top) and ¹⁵[2]³⁺ → ¹⁵[2]²⁺ (bottom) redox conversions in acetonitrile, $I = 1$ M (TBAPF₆). See the experimental section for details. The arrows indicate the spectral changes upon reduction.

between free and coordinated NO than the one computed in [2]³⁺. The diminished M-NO orbital interaction results also in a smaller d_{Ru}-π^*_{L2} energy gap, that reflects in the position and intensity of the low energy absorption bands in the visible region of the spectrum (Table 6 and Figure 5).

The experimental half wave potentials registered for the {RuNO}⁶/{RuNO}⁷ couples from CV, SWV or spectroelectrochemistry experiments performed employing solutions of [2]³⁺ turned to be independent of the pH in the acidic range. The same result was obtained when the redox conversion was explored employing solutions of [2]²⁺ prepared by 1-electron reduction of [2]³⁺ under spectroelectrochemical conditions. However, once the concentration of OH⁻ becomes high enough to promote the conversion to the nitro derivatives [1]⁺ (eq 2), no reduction of the latter could be detected at all, though anodic SWV scans of [2]²⁺ solutions displayed pH-dependent signals due to the coupled electrochemical oxidation to [2]³⁺ followed by chemical conversion of the latter to the nitro species in the time scale of the experiment. The pH-dependence of the signals is consistent (at least in the region where the nitrosyl-to-nitro conversion is slow) with a 1e⁻/2H⁺ process.

The {RuNO}⁷ to {RuNO}⁸ Conversion. CV measurements of acetonitrile solutions of [2]²⁺ at more cathodic potentials revealed a second reversible wave at −0.44 V (Figure 3). Figure 8 displays the spectral evolution in the UV−vis and IR spectroelectrochemical experiments, recorded with an applied potential of −0.65 V. The global analysis of the electronic spectra is again consistent with a 1-electron reduction process involving only two colored species that convert reversibly into each other with $E° = -0.46$ V. The electronic spectrum of the reduced species [2]⁺ consists of strong absorptions at 298 nm ($\varepsilon = 1.82 \times 10^4$ M⁻¹ cm⁻¹), 356 nm ($\varepsilon = 3.06 \times 10^3$ M⁻¹ cm⁻¹) and 480 nm ($\varepsilon = 3.56 \times 10^3$ M⁻¹ cm⁻¹). The evolution of the IR spectra along the electrochemical reduction reveals the disappearance of the v_{NO} vibration associated with the {RuNO}⁷ moiety, in parallel with the growth of two signals
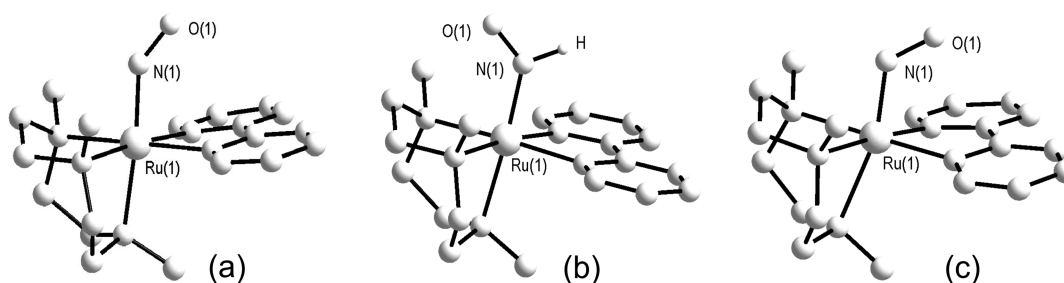
**Figure 7.** Optimized geometries obtained in the DFT optimization of (a) $[\mathbf{2}]^{2+}$, (b) $[\mathbf{2\text{-}H}]^{2+}$ and (c) $[\mathbf{2}]^{+}$.
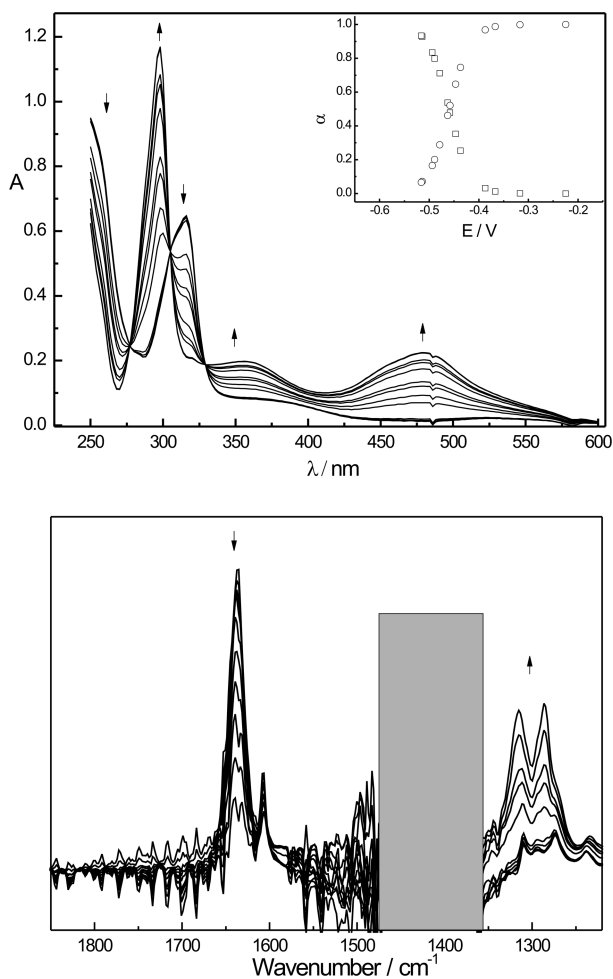

Figure 8. UV−vis (top) and IR (bottom) spectroelectrochemical reduction of $[\mathbf{2}]^{2+}$ in acetonitrile. See the Experimental Section for details. The inset in the top panel corresponds to the fraction of $[\mathbf{2}]^{2+}$ (circles) and $[\mathbf{2}]^{+}$ (squares) along the spectroelectrochemistry.

at 1315 and 1286 cm^{-1} (1290 and 1282 cm^{-1} for $^{15}[\mathbf{2}]^{2+}$). To our knowledge there are no examples of structurally (X-ray) characterized pairs of {MNO}^{7} and {MNO}^{8} species based on the same coordination sphere.[94] However, a shift of ~300 cm^{-1} has been already observed in the {MNO}^{7} → {MNO}^{8} conversion of $[\mathrm{Fe(NO)(cyclam\text{-}ac)}]^+$ in the same medium,[66] suggesting that the redox process represented by eq 9 leads to the analogous {RuNO}^{8} moiety.

$$[\mathrm{Ru(Me_3[9]aneN_3)(bpy)(NO)}]^{2+} + e^-$$

$$\rightarrow [\mathrm{Ru(Me_3[9]aneN_3)(bpy)(NO)}]^+ \qquad (9)$$
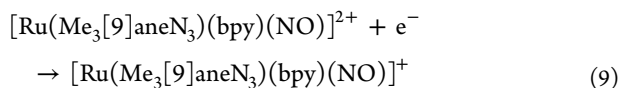
An analogous reduction step is also observable in water, although in this medium the process seems to be electrochemically irreversible on the CV time scale (Figure 3, top). Nevertheless, controlled potential coulometry of solutions of $[\mathbf{2}]^{2+}$ at pH 2.50 rendered chemically reversible 1-electron conversions between two colored species, as revealed in the electronic spectra of Figure 9. In contrast with the behavior observed in the {RuNO}^{6}/{RuNO}^{7} process, the spectral changes recorded in aqueous acidic solutions and in organic media are noticeably different. In water at pH 2.50, the electronic spectrum of the species obtained by 1-electron reduction of $[\mathbf{2}]^{2+}$ shows intense bands at 258 nm ($\varepsilon = 1.41 \times 10^4$ M^{-1} cm^{-1}), 302 nm ($\varepsilon = 1.14 \times 10^4$ M^{-1} cm^{-1}), 318 nm ($\varepsilon = 1.14 \times 10^4$ M^{-1} cm^{-1}), and 376 nm ($\varepsilon = 5.67 \times 10^3$ M^{-1} cm^{-1}). Such a difference in number, position and intensity of the bands cannot be solely attributed to solvatochromism, and is probably an indication that the aqueous species differs from the one in acetonitrile. Modification of the pH at which this redox process is explored reveals changes in the half-wave potential of the couple of ~60 mV per pH unit. This observation is independent of the experimental technique employed in the exploration (SWV or spectroelectrochemistry). The evidence suggests that the second redox step recorded in water corresponds to a proton-coupled 1-electron reduction as described by eq 10.

$$[\mathrm{Ru(Me_3[9]aneN_3)(bpy)(NO)}]^{2+}$$

$$+ e^- + H^+ \rightarrow [\mathrm{Ru(Me_3[9]aneN_3)(bpy)(HNO)}]^{2+}$$

$$(10)$$
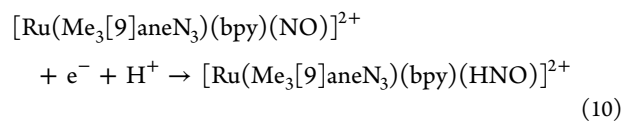
We performed a DFT exploration of the HNO holding species, similar to the one described above for the {RuNO}^{7} compound. The most remarkable structural differences with the computed geometry of the {RuNO}^{7} species are a lengthening of the N(1)−O(1) and Ru−N(1) bond lengths of ~0.06 and 0.03 Å, respectively, and a more pronounced bending of the Ru−N(1)−O(1) fragment to reach an angle close to 140°. These changes are consequences of the addition of an electron in an antibonding orbital of the coordinated ligand. There is no substantial change in the Ru−N(2) bond length, suggesting that, in agreement with other computational studies,[95] the HNO fragment does not induce a strong σ-trans effect. The rest of the coordination sphere remained roughly unaltered and deserves no further comment. The ν_{NO} stretching vibrations associated with the HNO fragment show up in a rather crowded region of the spectra strongly overlapped and combined with bpy-centered vibrations. Several modes in the fingerprint region have detectable N−O contributions. The vibrational mode computed at 1376 cm^{-1} is the one with the largest NO character. As a comparison, the computed N−O bond length and ν_{NO} obtained at exactly the same level of
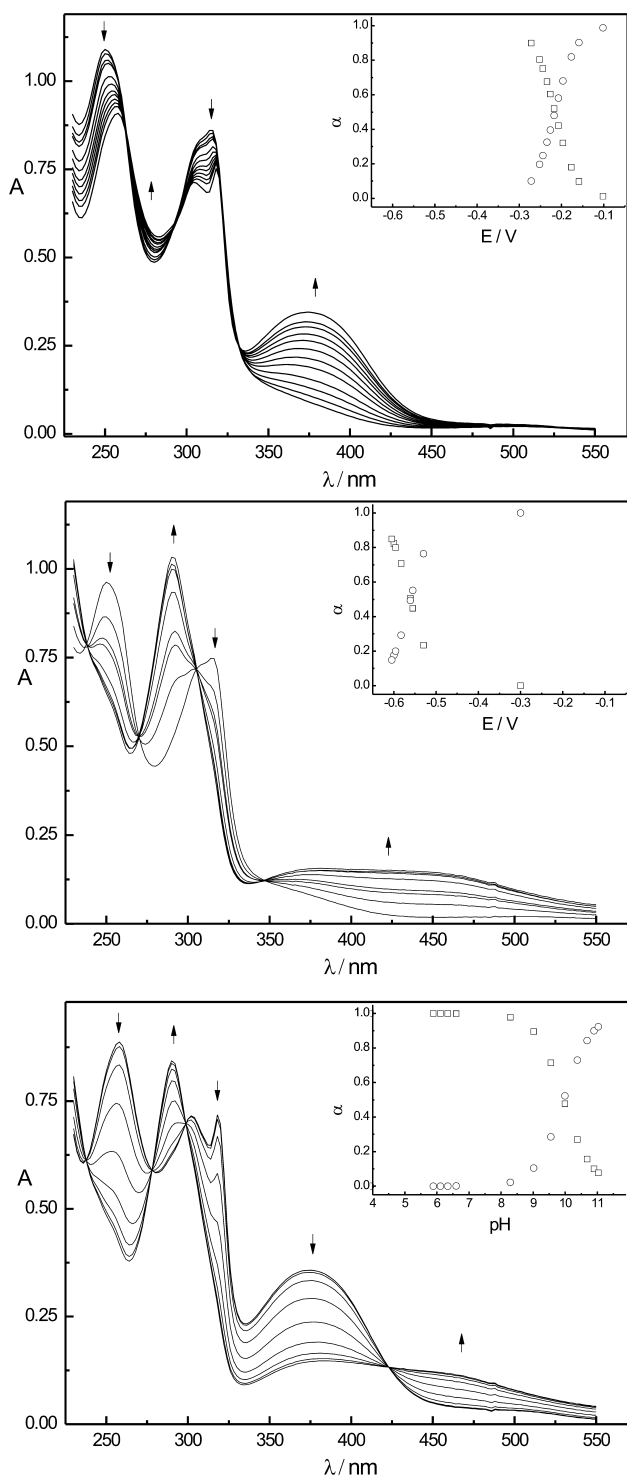
Figure 9. Spectroelectrochemical reduction of $[2]^{2+}$ in water, top panel: pH = 2.50 (phosphate), I = 1 M (NaCl). Middle: pH = 12.8 (NaOH), I = 1 M (NaCl). Bottom: Acid/base titration of $[2]^+$. See the Experimental Section for details.

theory for the free HNO molecule are 1.25 Å and 1483 cm^{-1} (Supporting Information, Table S2), respectively. The longer N−O bond length and lower ν_{NO} (a reduction of ∼9%) value computed upon coordination are consistent with a moderate π-backbonding from the metal center comparable to the one described in the {RuNO}^{7} species. Values around 1380 cm^{-1} assigned to ν_{NO} have been found also for related metallo—

nitroxyl complexes[10,33,36,37,96] and in a series of nitroso-adducts containing $(N(O)L)^n$ ligands bound to M(II) centers (M = Fe, Ru), with L = thiolate, sulfide, etc., reflecting a double bond character in the nitrosyl group.[97]

Consistently, the MO picture (Figure 10) reveals the t_{2g} set of d_{Ru} orbitals contributing to the HOMO, HOMO−1, and HOMO−2 orbitals. The contribution of HNO-centered orbitals to the HOMO and HOMO−1 is small (∼4%). The HOMO−2 comprises a large contribution from both Ru- and HNO-centered orbitals (63% and 21%) resulting from the Ru−HNO backbonding. The HOMO−3 is σ-bonding with respect to the HNO and the axial nitrogen atom trans to the HNO with substantial contribution (70%) from the filled π^* orbital of the HNO moiety. The lowest unoccupied MOs feature an empty orbital, mainly HNO−π^* in character, a set of empty bpy-centered orbitals, and the two e_g-like, mostly metal-centered orbitals. The strong spectral overlap prevents a clean assignment of the whole electronic spectrum. The computed spectrum is nevertheless in good agreement with the experimental one, supporting the theoretical analysis. According to these computations, the lowest energy absorption bands are mostly $d_{Ru} \rightarrow$ bpy MLCT bands. The (TD)DFT analysis also suggests the possibility of MLCT transitions involving the HNO-centered LUMO of the molecule, but unfortunately these bands are not clearly resolved in the experimental spectra.

In spite of its early reputation,[13] the species containing a coordinated HNO is not water sensitive and is in fact remarkably inert toward substitution. This has also been recently observed for $[Fe(CN)_5HNO]^{3-}$[37,40] and for Mb^{II}HNO.[13] No signs of decomposition could be detected in solutions well preserved from the air, and eventually the fully oxidized $[2]^{3+}$ (or $[1]^+$, depending on the pH) species were completely recovered electrochemically in two-step processes with intermediate formation of $[2]^{2+}$ after periods as long as 24 hs.

In the alkaline region the redox potential becomes independent of $[H^+]$. Spectroelectrochemistry yields also remarkably different spectral changes compared to the ones described at pH 2.5. Figure 9 (middle) displays the spectra recorded along the 1-electron reduction of $[2]^{2+}$ at pH 12.8. The spectral evolution is consistent with the appearance of a species with maxima at 290 nm (ε = 1.37 × 10^4 M^{-1} cm^{-1}), 374 nm (ε = 2.02 × 10^3 M^{-1} cm^{-1}), and 440 nm (ε = 2.07 × 10^3 M^{-1} cm^{-1}). Even when in water the absorption bands in the visible region are not as well resolved as in organic medium, the general aspect of the absorption profile resembles the one described in acetonitrile. This fact, combined with the pH independence of the process (Figure 11) suggests a conversion to $[2]^+$ as in eq 9.

The DFT-optimized geometry for $[2]^+$ shows an N(1)−O(1) bond length comparable to the one observed in the protonated species, but the Ru−N(1) distance is 0.02 Å shorter. There are more remarkable structural changes when comparing both molecules: $[2]^+$ has a more pronounced Ru−N(1)−O(1) bending, which reaches a value close to 120°, in agreement with comparatively greater repulsions arising from the presence of the lone pair at nitrogen. The Ru−N(2) bond length has a value of 2.41 Å (i.e., 0.19 Å longer than in $[2]^{2+}$ or $[2\text{-H}]^{2+}$) and the N(1)−Ru−N(2) angle of 164.8° deviates largely from linearity. Overall, the structural features point to a strong trans effect exerted by the coordinated NO$^-$.[27] The molecular orbital picture is consistent with an NO$^-$ moiety behaving as a donor fragment involving its HOMO-electrons
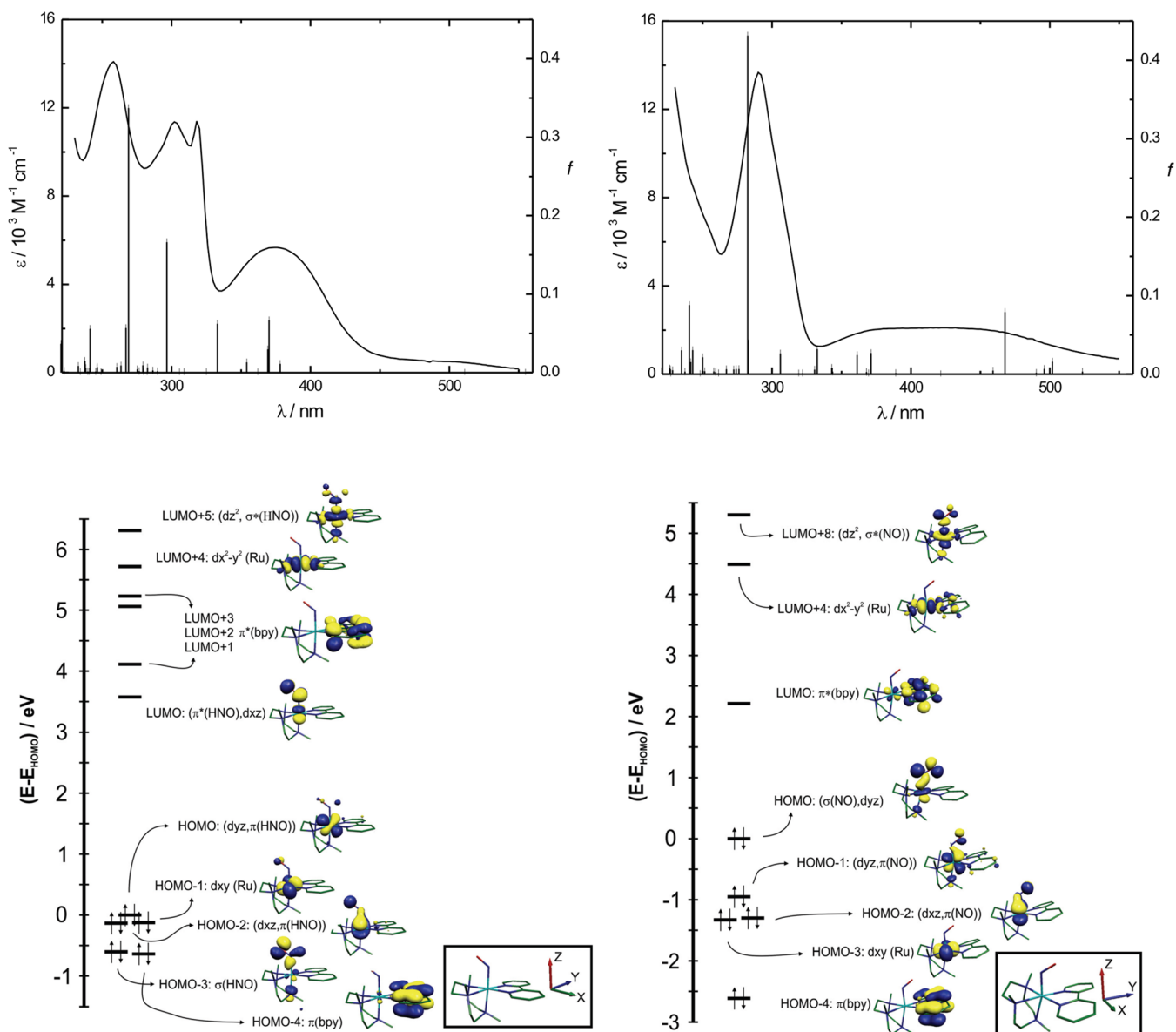
Figure 10. Experimental and (TD)DFT computed UV–vis spectra of $[2\text{-}H]^{2+}$ in water at pH = 2.50 (top, left) and $[2]^+$ in water at pH = 13.0 (top right), along with the molecular orbital diagrams for $[2\text{-}H]^{2+}$ (bottom, left) and $[2]^+$ (bottom, right).
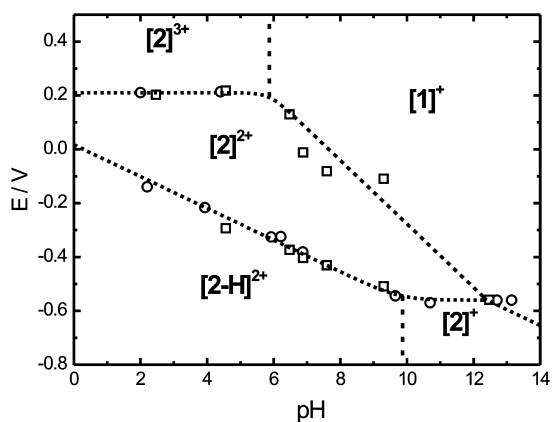

Figure 11. Potential $(E_{1/2})$ − pH diagram showing the redox and acid–base behavior of the systems described in this manuscript. Data arising from SWV experiments are displayed as squares, while those originating from the spectroelectrochemistry are represented as circles.

that reside in a π orbital mostly located on the N atom, antibonding with respect to the N−O bond. The computed vibrational mode with the highest NO character shows up at 1404 cm^{-1} (1379 cm^{-1} for $[^{15}2]^+$), somewhat higher than that obtained experimentally in acetonitrile. Due to the fact that DFT methods with standard functionals tend to provide too delocalized molecular and electronic structures due to inherent self-interaction errors,[98] the π-donor behavior of the NO$^-$ moiety might be overestimated influencing the computed ν_{NO}. Because of the lack of experience calculating this kind of system at the same level of theory, it is hard to establish the accuracy of the electronic description arising from the DFT computations. However, the changes observed in the geometry and the pictures of the qualitative electronic structure are most probably correct.

Combined Redox and Acid−Base Information: A Potential ($E_{1/2}$) − pH Diagram of the System. Figure 11 collects the redox information discussed in the previous sections in a complete Pourbaix-like diagram, which to our

knowledge represents the first thermodynamic description of such an important set of five nitrogenated species in aqueous solution. The different regions of stability for the $\{RuNO\}^n$ species are clearly defined. The line that separates the $n = 7$ from $n = 8$ compounds breaks at a pH close to 10, indicating that the coordinated HNO can engage in acid−base processes as described in eq 11.

$$[Ru(Me_3[9]aneN_3)(bpy)(HNO)]^{2+}$$
$$\rightleftharpoons [Ru(Me_3[9]aneN_3)(bpy)(NO)]^+ + H^+ \qquad (11)$$
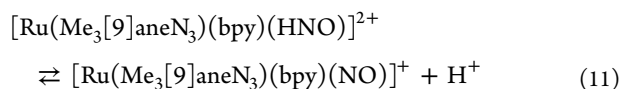
It is worth noting that, according to this diagram, $[2]^{2+}$ should be unstable toward disproportionation at pH above 12.3, as described by eq 12:

$$2[Ru(Me_3[9]aneN_3)(bpy)(NO)]^{2+} + H_2O$$
$$\rightarrow [Ru(Me_3[9]aneN_3)(bpy)(NO)]^+$$
$$+ [Ru(Me_3[9]aneN_3)(bpy)(NO_2)]^+ + 2H^+ \qquad (12)$$
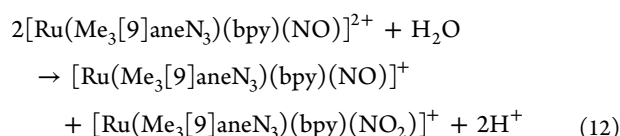
However, as stated before, the solutions remain unchanged in basic medium. Moreover, the $[2]^{2+}/[2]^+$ conversion can be still explored, yielding the appropriate products and pH-independent half-wave potential values (see Figure 11). There is probably an activation barrier for reaction 12, an issue that prompts further investigations.

The quantitative estimation of the pK_a for the process described by eq 11 is of fundamental interest. The kinetic barrier arising from the different spin multiplicities of free ^1HNO and its conjugated base $^3NO^-$ has been invoked to warn about the real significance of the pK_a values. Deprotonation of free ^1HNO requires a spin flip, thus making the proton transfer process slow.[11,13] However, bound NO^- (as O_2) is a singlet species.[26,66] In the absence of a kinetic barrier due to a change in the spin multiplicity between bound HNO and NO^- the behavior is the same as the one described in any regular conjugated acid−base pair. We explored the following three ways to extract the pK_a value in the bound system from the combined redox and acid−base data: (i) Intersection of the lines that represent the pH-dependence of the half-wave potentials for $[2]^{2+}/[2]^+$ and $[2]^{2+}/[2\text{-}H]^{2+}$ couples. (ii) Global analysis of whole sets of E and pH-dependent spectra recorded along the spectroelectrochemical exploration of the system, considering the presence of three colored species ($[2]^{2+}$, $[2]^+$, and $[2\text{-}H]^{2+}$) linked by eqs 9−11. (iii) UV−vis-monitored titration with base of a solution of $[2\text{-}H]^{2+}$ obtained under controlled potential coulometry in the acidic range, followed by a multiwavelength treatment of the experimental data (Figure 9, bottom). The three procedures rendered virtually the same results and an average pK_a of 9.78 ± 0.15. This number is much lower than 23, the estimated value for the free HNO $\rightleftharpoons {}^1NO^-$ + H$^+$ conversion (the value is 11.5 for $^3NO^-$).[39] The expected increased acidity upon coordination is probably influenced by the stabilization of the conjugated base due to the donating properties of NO^- toward the metal center, already revealed by the MO computations. For the sake of comparison, the value is consistent with the robust properties and persistence of the ^1H NMR signal observed for $Mb^{II}HNO$ up to pH 10.[36] On the other hand, this pK_a is significantly higher than the previous report of 7.7 for $[Fe(CN)_5(HNO)]^{3-}$ in aqueous solution,[37] an unexpected result provided that the negatively charged $[Fe(CN)_5]^{3-}$ moiety should be a poorer Lewis acid than $[Ru(Me_3[9]aneN_3)(bpy)]^{2+}$. At this point we can only

speculate about the possible origin of this discrepancy, though we should remark that the trans labilization promoted by the NO^- group could be strongly enhanced in $[Fe(CN)_5(NO)]^{4-}$, thus suggesting that the measured pK_a might in fact be an apparent value reflecting other complications aside from the proton release, while the same effect appears to be hindered by chelation at the trans position in $[Ru(Me_3[9]aneN_3)(bpy)\text{-}(NO)]^+$. In fact, elucidating the speciation of bound NO, NO^-, and HNO, as done in this work, has a great bioinorganic relevance, given the possible role of these species in the relevant media. Given the different physiological roles of NO and "nitroxyl",[11] the real predominance of NO^- or HNO (each with a characteristic reactivity) becomes also crucial.[12]

■ CONCLUSIONS AND PROSPECT

The new $[Ru(Me_3[9]aneN_3)(bpy)(NO)]^{3+}$ compound proved to be a valuable platform to investigate the combined acid−base and redox chemistries in $\{RuNO\}^{6,7,8}$ species. The marked inertness of the coordination sphere for the three oxidation states and the color changes associated with the acid−base and the redox conversions opened the possibility to thoroughly explore the structural picture with high accuracy, employing simple experimental tools, and allow for further investigation of the relevant chemistry. The results suggest that NO, NO^-, and HNO can be stabilized and handled over long periods of time and varying conditions if the lability of the coligand environment can be kept under control. The abundant experience in connection with the derivatization of $[9]aneN_3$ and bpy envisages many possible variations by using coligands with different donor/acceptor capabilities, thus enabling for a systematic exploration of the factors that could influence the acid−base properties of coordinated HNO. The use of theoretical approaches as employed here are interesting tools to interpret the tendencies and eventually might be of significant help in the selection of the appropriate substituents to fine-tune the desired properties. Above all, this system reveals as an interesting platform to perform fundamental reactivity studies on related $\{MNO\}^{6,7,8}$ compounds. Among the possibilities, the reaction of $\{RuNO\}^{7,8}$ with O_2 is of great relevance.[99] The same comment applies to the photochemistry of the reduced $\{MNO\}^{7,8}$ species, which unlike the case of the $\{MNO\}^6$ compounds,[55,100] has been only partially studied and requires a further systematic exploration.[101] We are currently investigating these possibilities

■ ASSOCIATED CONTENT

ⓢ Supporting Information

IR and NMR spectra (with signal assignments) of $[1]^+$ and $[2]^{3+}$; time evolution pH dependency and k_{obs} vs $[OH^-]$ for the reaction between $[2]^{3+}$ and OH^-; comparison between the electronic spectra of $[1]^+$ and $[2]^{3+}$ in water and acetonitrile; structural parameters obtained from DFT computations for $[1]^+$, $[2]^{3+}$, $[2]^{2+}$, $[2\text{-}H]^{2+}$ and $[2]^+$; correlation between experimental and computed vibrational frequencies in $[1]^+$ and $[2]^{3+}$; experimental and computed properties of free and coordinated NO^+, NO, NO^-, and HNO; DFT-computed MO orbitals and (TD)DFT electronic transitions for $[1]^+$, $[2]^{3+}$, $[2]^{2+}$, $[2\text{-}H]^{2+}$ and $[2]^+$; spin density plot for $[2]^{2+}$; crystallographic information files. This material is available free of charge via the Internet at http://pubs.acs.org.

■ AUTHOR INFORMATION

Corresponding Author
*E-mail: slep@qi.fcen.uba.ar

Notes
The authors declare no competing financial interest.

■ REFERENCES

(1) Richter-Addo, G. B.; Legzdins, P. *Metal Nitrosyls*; Oxford University Press: New York, 1992.

(2) Olabe, J. A.; Slep, L. D. Reactivity and Structure of Complexes of Small Molecules: Nitric and Nitrous Oxide. In *Comprehensive Coordination Chemistry II, from Biology to Nanotechnology*; McCleverty, J. A., Meyer, T. J., Eds.; Elsevier: Oxford, 2004; Vol. 1, pp 603−623.

(3) McCleverty, J. A. *Chem. Rev.* **2004**, *104*, 403−418.

(4) Roncaroli, F.; Videla, M.; Slep, L. D.; Olabe, J. A. *Coord. Chem. Rev.* **2007**, *251*, 1903−1930.

(5) (a) Ignarro, J. L. E. *Nitric Oxide, Biology and Pathobiology*; Academic Press: San Diego, CA, 2000. (b) Moncada, S.; Palmer, R. M. P.; Higgs, E. A. *Pharmacol. Rev.* **1991**, *43*, 109−142.

(6) Stone, J. R.; Marletta, M. A. *Biochemistry* **1994**, *33*, 5636−5640.

(7) Stuehr, D. J.; Kwon, N. S.; Nathan, C. F.; Griffith, O. W.; Feldman, P. L.; Wiseman, J. *J. Biol. Chem.* **1991**, *266*, 6259−6263.

(8) (a) Eady, R. R.; Hasnain, S. S. Denitrification. In *Comprehensive Coordination Chemistry II, from Biology to Nanotechnology*; McCleverty, J. A., Meyer, T. J., Eds.; Elsevier: Oxford, 2004; Vol. 8, pp 759−786; (b) Lee, D. H.; Mondal, B.; Karlin, K. D. In *Activation of Small Molecules*; Tolman, W., Ed.; Wiley-VCH, 2006.

(9) Wasser, I. M.; de Vries, S.; Moenne-Loccoz, P.; Schroder, I.; Karlin, K. D. *Chem. Rev.* **2002**, *102*, 1201−1234.

(10) Averill, B. A. *Chem. Rev.* **1996**, *96*, 2951−2964.

(11) (a) Paolocci, N.; Jackson, M. I.; Lopez, B. E.; Miranda, K.; Tocchetti, C. G.; Wink, D. A.; Hobbbs, A. J.; Fukuto, J. M. *Pharmacol. Ther.* **2007**, *113*, 442−458. (b) Fukuto, J. M.; Cisneros, C. J.; Kinkade, R. L. *J. Inorg. Biochem.* **2013**, *118*, 201−208.

(12) Miranda, K. M. *Coord. Chem. Rev.* **2005**, *249*, 433−455.

(13) Farmer, P. J.; Sulc, F. *J. Inorg. Biochem.* **2005**, *99*, 166−184.

(14) (a) Doctorovich, F.; Bikiel, D. E.; Pellegrino, J.; Suárez, S. A.; Martí, M. A. *Adv. Inorg. Chem.* **2012**, *64*, 97−139. (b) Doctorovich, F.; Bikiel, D. E.; Pellegrino, J.; Suárez, S. A.; Larsen, A.; Martí, M. A. *Coord. Chem. Rev.* **2011**, *255*, 2764.

(15) Goodrich, L. E.; Paulat, F.; Praneeth, V. K. K.; Lehnert, N. *Inorg. Chem.* **2010**, *49*, 6293−6316.

(16) Enemark, J. H.; Feltham, R. D. *Coord. Chem. Rev.* **1974**, *13*, 339−406. Enemark, J. H.; Feltham, R. D. *Top. Stereochem.* **1981**, *12*, 155−215.

(17) Structures of metallonitrosyls are currently described in terms of the Enemark−Feltham formalism (ref 16) {MNO}^{n}, with n standing for the total number of d electrons occupying either metal- or π_{NO*} orbitals. This description is valid for different coordination numbers, without specifying the identity of the coligands. In this context, the detailed electronic distribution in the MNO moieties cannot be anticipated by the different values of n; instead, it must be carefully assigned by employing a combined approach, using different spectroscopic measurements (X-ray, IR, NMR, EPR, MCD, etc., and/or theoretical calculations). Therefore, assignments with formal oxidation states at the metal or nitrosyl ligands (viz., NO$^+$, NO$^\bullet$, NO$^-$) are extreme descriptions that need to be adequately modified according to the above indicators (namely, for $n = 6$, Fe^{II}NO$^+$ may be dominant, although a sizable contribution of Fe^{III}NO$^\bullet$ could be considered; similarly for $n = 7$, with Fe^{II}NO$^\bullet$, Fe^{III}NO$^-$, or Fe^{I}NO$^+$, and so on).

(18) (a) Silvernail, N. J.; Pavlik, J. W.; Noll, B. C.; Schulz, C. E.; Scheidt, R. *Inorg. Chem.* **2008**, *47*, 912−920. (b) Schoonover, M. W.; Baker, E. C.; Eisenberg, R. *J. Am. Chem. Soc.* **1979**, *101*, 1880−1882.

(19) Hannibal, L.; Smith, C. a.; Jacobsen, D. W.; Brasch, N. E. *Angew. Chem., Int. Ed.* **2007**, *46*, 5140−5143.

(20) Cámpora, J.; Palma, P.; del Río, D.; Carmona, E.; Graiff, C.; Tiripicchio, A. *Organometallics* **2003**, *22*, 3345−3347.

(21) Lanfranchi, M.; Tiripicchio, A.; Giuliano, G.; Ghedini, M. *Transition Met. Chem.* **1980**, *5*, 21−25.

(22) Kelly, B. A.; Welch, A. J.; Woodward, P. *J. Chem. Soc., Dalton Trans.* **1977**, 2237.

(23) Enemark, J. H.; Feltham, R. D.; Riker-Nappier, J.; Bizot, K. F. *Inorg. Chem.* **1975**, *14*, 624−632.

(24) Weaver, D. L.; Snyder, D. A. *Inorg. Chem.* **1970**, *9*, 2760−2767.

(25) (a) Lancon, D.; Kadish, K. M. *J. Am. Chem. Soc.* **1983**, *105*, 5610−5617. (b) Choi, I. K.; Liu, Y.; Feng, D. W.; Paeng, K. J.; Ryan, M. D. *Inorg. Chem.* **1991**, *30*, 1832−1839. (c) Wei, Z.; Ryan, M. D. *Inorg. Chem.* **2010**, *49*, 6948−6954.

(26) Pellegrino, J.; Bari, S. E.; Bikiel, D. E.; Doctorovich, F. *J. Am. Chem. Soc.* **2010**, *132*, 989−995.

(27) Goodrich, L. E.; Roy, S.; Alp, E. E.; Zhao, J.; Hu, M. Y.; Lehnert, N. *Inorg. Chem.* **2013**, *52*, 7766−7780.

(28) Patra, A. K.; Dube, K. S.; Sanders, B. C.; Papaefthymiou, G. C.; Conradie, J.; Ghosh, A.; Harrop, T. C. *Chem. Sci.* **2012**, *2*, 364−369.

(29) Wilson, R. D.; Ibers, J. A. *Inorg. Chem.* **1979**, *18*, 336−343.

(30) Melenkivitz, R.; Hillhouse, G. L. *Chem. Commun.* **2002**, *2*, 660−661.

(31) Sellmann, D.; Gottschalk-Gaudig, T.; Haussinger, D.; Heinemann, F. W.; Hess, B. A. *Chem.—Eur. J.* **2001**, *7*, 2099−2103.

(32) (a) Southern, J. S.; Hillhouse, G. L.; Rheingold, A. L. *J. Am. Chem. Soc.* **1997**, *119*, 12406−12407. (b) Song, W.; Ellern, A.; Bakac, A. *Inorg. Chem.* **2008**, *47*, 8405−8411. (c) Levina, A.; Turner, P.; Lay, P. A. *Inorg. Chem.* **2003**, *42*, 5392−5398. (d) Ardon, M.; Cohen, S. *Inorg. Chem.* **1993**, *32*, 3241−3243.

(33) Melenkivitz, R.; Southern, J. S.; Hillhouse, G. L.; Concolino, T. E.; Liable-Sands, L.; Rheingold, A. L. *J. Am. Chem. Soc.* **2002**, *124*, 12068−12069.

(34) Pratt, C. S.; Coyle, B. A.; Ibers, J. A. *J. Chem. Soc. (A)* **1971**, 2146−2151.

(35) Schaniel, D.; Woike, T.; Behrnd, N.-R.; Hauser, J.; Krämer, K. W.; Todorova, T.; Delley, B. *Inorg. Chem.* **2009**, *48*, 11399−11406.

(36) Lin, R.; Farmer, P. J. *J. Am. Chem. Soc.* **2000**, *122*, 2393−2394.

(37) Montenegro, A. C.; Amorebieta, V. T.; Slep, L. D.; Martin, D. F.; Roncaroli, F.; Murgida, D. H.; Bari, S. E.; Olabe, J. A. *Angew. Chem., Int. Ed.* **2009**, *48*, 4213−4216.

(38) Gratzel, M.; Taniguchi, S.; Henglein, A. *Ber. Bunsen-Ges. Phys. Chem.* **1979**, *74*, 1003.

(39) (a) Bartberger, M. D.; Liu, W.; Ford, E.; Miranda, K.; Switzer, C.; Fukuto, J. M.; Farmer, P. J.; Wink, D. A.; Houk, K. N. *Proc. Natl. Acad. Sci. U.S.A.* **2002**, *99*, 10958−10963. (b) Shafirovich, V.; Lymar, S. V. *Proc. Natl. Acad. Sci. U.S.A.* **2002**, *99*, 7340.

(40) Montenegro, A. C.; Bari, S. E.; Olabe, J. A. *J. Inorg. Biochem.* **2013**, *118*, 108−114.

(41) Armarego, W. L. F.; Perrin, D. D. *Purification of Laboratory Chemicals*; Reed Educational & Professional Publishing Ltd.: Oxford, 1996.

(42) Cheng, W. C.; Yu, W. Y.; Cheung, K. K.; M., C. C. *J. Chem. Soc., Dalton Trans* **1994**, 57−62.

(43) Malinovsky, E. R. *Factor Analysis in Chemistry*, 2nd ed.; Wiley-Interscience: New York, 1991.

(44) Slep, L. D.; Mijovilovich, A.; Meyer-Klaucke, W.; Weyhermuller, T.; Bill, E.; Bothe, E.; Neese, F.; Wieghardt, K. *J. Am. Chem. Soc.* **2003**, *125*, 15554−15570.

(45) Krejcik, M.; Danek, M.; Hartl, F. *J. Electroanal. Chem.* **1991**, *317*, 179.

(46) Roncaroli, F.; Baraldo, L. M.; Slep, L. D.; Olabe, J. A. *Inorg. Chem.* **2002**, *41*, 1930−1939.

(47) *SADABS*, 2006/1; Bruker AXS Inc.: Madison, WI, U.S.A., 2007.

(48) *ShelXTL*, 6.14; Bruker AXS Inc.: Madison, WI, U.S.A., 2003.

(49) Sheldrick, G. M. *ShelXL97*; University of Göttingen: Göttingen, Germany, 1997.

(50) Frisch, M. J.; et al. *Gaussian 03*, Rev. C.02 and D.01; Gaussian Inc.: Wallingford CT, 2004.

(51) (a) Becke, A. D. *J. Chem. Phys.* **1988**, *84*, 4524−4529. (b) Becke, A. D. *J. Chem. Phys.* **1993**, *98*, 5648−5652. (c) Lee, C.; Yang, W.; Parr, R. G. *Phys. Rev. B* **1988**, *37*, 785−789. (d) Perdew, J. P. *Phys. Rev. B* **1986**, *33*, 8822−8824.

(52) (a) Dunning, T. H., Jr.; Hay, P. J. Modern Theoretical Chemistry. In *Modern Theoretical Chemistry*; Schaefer, H. F., III., Ed.; Plenum: New York, NY, 1976; pp 1−28; (b) Hay, P. J.; Wadt, W. R. *J. Chem. Phys.* **1985**, *82*, 270−283. (c) Hay, P. J.; Wadt, W. R. *J. Chem. Phys.* **1985**, *82*, 299−310. Wadt, W. R.; Hay, P. J. *J. Chem. Phys.* **1985**, *82*, 284−298.

(53) (a) Armor, J.; Hoffman, M. *Inorg. Chem.* **1975**, *14*, 444−446. (b) Gomes, M. G.; Davanzo, C. U.; Silva, S. C.; Lopez, L. G. F.; Santos, P. S.; Franco, D. W. *J. Chem. Soc., Dalton Trans.* **1998**, *4*, 601−607. (c) Borges, S. S. S.; Davanzo, C. U.; Castellano, E. E.; Z-Schpector, J.; Silva, S. C.; Franco, D. W. *Inorg. Chem.* **1998**, *37*, 2670−2677. (d) Tfouni, E.; Ferreira, K. Q.; Doro, F. G.; da Silva, R. S.; da Rocha, Z. N. *Coord. Chem. Rev.* **2005**, *249*, 405−418.

(54) Gorelsky, S. I.; da Silva, S. C.; Lever, A. B. P.; Franco, D. W. *Inorg. Chim. Acta* **2000**, *300*, 698−708.

(55) Tfouni, E.; Krieger, M.; McGarvey, B. R.; Franco, D. W. *Coord. Chem. Rev.* **2003**, *236*, 57−69.

(56) Lang, D. R.; Davis, J. A.; Lopes, L. G. F.; Ferro, A. A.; Vasconcellos, L. C. G.; Franco, D. W.; Tfouni, E.; Wieraszko, A.; Clarke, M. J. *Inorg. Chem.* **2000**, *39*, 2294−2300.

(57) Roncaroli, F.; Ruggiero, M. E.; Franco, D. W.; Estiu, G. L.; Olabe, J. A. *Inorg. Chem.* **2002**, *41*, 5760−5769.

(58) Freedman, D. A.; Janzen, D. E.; Mann, K. R. *Inorg. Chem.* **2001**, *40*, 6009−6016.

(59) Freedman, D. A.; Kruger, S.; Roosa, C.; Wymer, C. *Inorg. Chem.* **2006**, *45*, 9558−9568.

(60) De, P.; Maji, S.; Chowdhury, A. D.; Mobin, S. M.; Mondal, T. K.; Paretzki, A.; Lahiri, G. K. *Dalton Trans.* **2011**, *40*, 12527−12539.

(61) Videla, M.; Jacinto, J. S.; Baggio, R.; Garland, M. T.; Singh, P.; Kaim, W.; Slep, L. D.; Olabe, J. A. *Inorg. Chem.* **2006**, *45*, 8608−8617.

(62) Li, J.; Noodleman, L.; Case, D. A. Electronic Structure Calculations with Applications to Transition Metal Complexes. In *Inorganic Electronic Structure and Spectroscopy*; Solomon, E. I., Lever, A. P. B., Eds.; Wiley, 1999; Vol. *1*, pp 661−724.

(63) De Candia, A. G.; Marcolongo, J. P.; Etchenique, R.; Slep, L. D. *Inorg. Chem.* **2010**, *49*, 6925−6930.

(64) Osa Codesido, N.; De Candia, A. G.; Weyhermuller, T.; Olabe, J. A.; Slep, L. D. *Eur. J. Inorg. Chem.* **2012**, 4301−4309.

(65) The DFT calculated spectra are shifted to lower wavenumbers by a multiplicative factor of 0.98 ± 0.01. This behavior is not unusual and has been already reported in other systems at the same level of computation

(66) Serres, R. G.; Grapperhaus, C. A.; Bothe, E.; Bill, E.; Weyhermuller, T.; Neese, F.; Wieghardt, K. *J. Am. Chem. Soc.* **2004**, *126*, 5138−5153.

(67) Slep, L. D.; Pollak, S.; Olabe, J. A. *Inorg. Chem.* **1999**, *38*, 4369−4371.

(68) Yi, G. B.; Khan, M. A.; Richter-Addo, G. B. *Inorg. Chem.* **1996**, *35*, 3453−3454.

(69) Bohle, D. S.; Hung, C. H.; Smith, B. D. *Inorg. Chem.* **1998**, *37*, 5798−5806.

(70) Miranda, K. M.; Bu, X. H.; Lorkovic, I.; Ford, P. C. *Inorg. Chem.* **1997**, *36*, 4838−4848.

(71) Yi, G. B.; Chen, L.; Khan, M. A.; Richter-Addo, G. B. *Inorg. Chem.* **1997**, *36*, 3876−3885.

(72) Scheidt, W. R.; Lee, Y. J.; Hatano, K. *J. Am. Chem. Soc.* **1984**, *106*, 3191−3198.

(73) Bottomley, F. *J. Chem. Soc., Dalton Trans.* **1974**, 1600−1605.

(74) Bezerra, C. W. B.; da Silva, S. C.; Gambardella, M. T. P.; Santos, R. H. A.; Plicas, L. M. A.; Tfouni, E.; Franco, D. W. *Inorg. Chem.* **1999**, *38*, 5660−5667.

(75) Lopes, L. G. F.; Wieraszko, A.; El-Sherif, Y.; Clarke, M. J. *Inorg. Chim. Acta* **2001**, *312*, 15−22.

(76) Nagao, H.; Nishimura, H.; Funato, H.; Ichikawa, Y.; Howell, F. S.; Mukaida, M.; Kakihana, H. *Inorg. Chem.* **1989**, *28*, 3955−3959.

(77) Olabe, J. A.; Gentil, L. A.; Rigotti, G. E.; Navaza, A. *Inorg. Chem.* **1984**, *23*, 4297−4302.

(78) Ellison, M. K.; Scheidt, W. R. *J. Am. Chem. Soc.* **1999**, *121*, 5210−5219.

(79) Ellison, M. K.; Schulz, C. E.; Scheidt, W. R. *Inorg. Chem.* **1999**, *38*, 100−108.

(80) Richter-Addo, G. B.; Wheeler, R. A.; Hixson, C. A.; Chen, L.; Khan, M. A.; Ellison, M. K.; Schulz, C. E.; Scheidt, W. R. *J. Am. Chem. Soc.* **2001**, *123*, 6314−6326.

(81) Hauser, C.; Glaser, T.; Bill, E.; Weyhermuller, T.; Wieghardt, K. *J. Am. Chem. Soc.* **2000**, *122*, 4352−4365.

(82) Sellmann, D.; Blum, N.; Heinemann, F. W.; Hess, B. A. *Chem.— Eur. J.* **2001**, *7*, 1874−1880.

(83) Pohl, K.; Wieghardt, K.; Nuber, B.; Weiss, J. *J. Chem. Soc., Dalton Trans.* **1987**, 187.

(84) Lopez, J. P.; Heinemann, F. W.; Prakash, R.; Hess, B. A.; Horner, O.; Jeandey, C.; Oddou, J. L.; Latour, J. M.; Grohmann, A. *Chem.—Eur. J.* **2002**, *8*, 5709−5722.

(85) De Candia, A. G.; Singh, P.; Kaim, W.; Slep, L. D. *Inorg. Chem.* **2009**, *48*, 565−573.

(86) De Candia, A. G.; Marcolongo, J. P.; Slep, L. D. *Polyhedron* **2007**, *26*, 4719−4730.

(87) Callahan, R. W.; Meyer, T. J. *Inorg. Chem.* **1977**, *16*, 574−581.

(88) Baraldo, L. M.; Bessega, M. S.; Rigotti, G. E.; Olabe, J. A. *Inorg. Chem.* **1994**, *33*, 5890−5896.

(89) Fuoss, R. M. *J. Am. Chem. Soc.* **1958**, *80*, 5059−5061.

(90) Wilkins, R. W. *Kinetics and Mechanism of Reactions of Transition Metal Complexes*, 2nd ed.; VCH: Weinheim, 1991.

(91) Bard, A. J.; Faulkner, L. R. *Electrochemical Methods, Fundamentals and Applications*; Wiley & Sons: New York, 1980.

(92) Bottomley, F.; Mukaida, M. *J. Chem. Soc., Dalton Trans.* **1982**, 1933−1937. Togano, T.; Kuroda, H.; Nagao, N.; Maekawa, Y.; Nishimura, H.; Howell, F. S.; Mukaida, M. *Inorg. Chim. Acta* **1992**, *196*, 57−63.

(93) Pipes, D. W.; Meyer, T. J. *Inorg. Chem.* **1984**, *23*, 2466−2472.

(94) *Cambridge Structural Database*; Cambridge Crystallographic Data Centre:Cambridge, England, 2013; www.ccdc.cam.ac.uk/conts/retrieving.html .

(95) Goodrich, L. E.; Lehnert, N. *J. Inorg. Biochem.* **2013**, *118*, 179−186.

(96) (a) Liochev, S. I.; Fridovich, I. *J. Biol. Chem.* **2001**, *276*, 35253−35257. (b) Liochev, S. I.; Fridovich, I. *Free Radical Biol. Med.* **2003**, *34*, 1399−1404.

(97) (a) Schwane, J. D.; Ashby, M. T. *Inorg. Chem.* **2002**, *124*, 6822−6823. (b) Quiroga, S. L.; Almaraz, A. E.; Amorebieta, V. T.; Perissinotti, L. L.; Olabe, J. A. *Chem.—Eur. J.* **2011**, *17*, 4145−4156.

(98) Cohen, A. J.; Mori-Sánchez, P.; Yang, W. *Science* **2008**, *321*, 792−794.

(99) (a) Ford, P. C.; Lorkovic, I. M. *Chem. Rev.* **2002**, *102*, 993−1017. (b) Ford, P. C.; Laverman, L. E.; Lorkovic, I. *Adv. Inorg. Chem.* **2003**, *54*, 203−257. (c) Videla, M.; Roncaroli, F.; Slep, L. D.; Olabe, J. A. *J. Am. Chem. Soc.* **2007**, *129*, 278−279.

(100) (a) Sauaia, M. G.; de Lima, R. G.; Tedesco, A. C.; da Silva, R. S. *Inorg. Chem.* **2005**, *44*, 9946−9951. (b) Sauaia, M. G.; de Lima, R. G.; Tedesco, A. C.; da Silva, R. S. *J. Am. Chem. Soc.* **2003**, *125*, 14718−14719. (c) Rose, M. J.; Patra, A. K.; Alcid, E. A.; Olmstead, M. M.; Mascharak, P. K. *Inorg. Chem.* **2007**, *46*, 2328−2338. (d) Rose, M. J.; Olmstead, M. M.; Mascharak, P. K. *Polyhedron* **2007**, *26*, 4713−4718. (e) Rose, M. J.; Mascharak, P. K. *Chem. Commun.* **2008**, 3933−3935. (f) Rose, M. J.; Mascharak, P. K. *Curr. Opin. Chem. Biol.* **2008**, *12*, 238−244. (g) Halpenny, G. M.; Mascharak, P. K. *Inorg. Chem.* **2009**,

996

dx.doi.org/10.1021/ic402448p | *Inorg. Chem.* 2014, 53, 981−997

48, 1490−1497. (h) Fry, N. L.; Rose, M. J.; Rogow, D. L.; Nyitray, C.; Kaur, M.; Mascharak, P. K. *Inorg. Chem.* **2010**, *49*, 1487−1495. (i) Ford, P. C.; Bourassa, J.; Miranda, K.; Lee, B.; Lorkovic, I.; Boggs, S.; Kudo, S.; Laverman, L. *Coord. Chem. Rev.* **1998**, *171*, 185−202. (j) Wolfe, S. K.; Swinehart, J. H. *Inorg. Chem.* **1975**, *14*, 1049−1053. (k) Videla, M.; Braslavsky, S. E.; Olabe, J. A. *Photochem. Photobiol. Sci.* **2005**, *4*, 75−82. (l) Togniolo, V.; da Silva, R. S.; Tedesco, A. C. *Inorg. Chim. Acta* **2001**, *316*, 7−12. (m) De Leo, M.; Ford, P. C. *J. Am. Chem. Soc.* **1999**, *121*, 1980−1981. (n) Adachi, H.; Sonoki, H.; Hoshino, M.; Wakasa, M.; Hayashi, H.; Miyazaki, Y. *J. Phys. Chem. A* **2001**, *105*, 392−398. (o) Fry, N. L.; Mascharak, P. K. *Acc. Chem. Res.* **2011**, *44*, 289−298. (p) Merkle, A. C.; Mc Quaters, A. B.; Lehnert, N. *Dalton Trans.* **2012**, *41*, 8047−8059.

(101) (a) Hoshino, M.; Ozawa, K.; Seki, H.; Ford, P. C. *J. Am. Chem. Soc.* **1993**, *115*, 9568−9575. (b) Laverman, L. E.; Wanat, A.; Oszajca, J.; Stochel, G.; Ford, P. C.; van Eldik, R. *J. Am. Chem. Soc.* **2001**, *123*, 285−293. (c) Ford, P. C. *Inorg. Chem.* **2010**, *49*, 6226−6239.